FROM HAYABUSA TO HAYABUSA2: PRESENT STATUS AND PLANS OF CURATORIAL WORKS FOR JAXA'S ASTEROIDAL SAMPLE RETURN MISSIONS.

T. Yada[1], K. Sakamoto[1], M. Yoshitake[1], K. Kumagai[2], M. Nishimura[2], K. Yogata[1], Y. Nakano[4], S. Furuya[1], M. Abe[1], T. Okada[1], S. Tachibana[3], H. Yurimoto[1,4], and M. Fujimoto[1,5], [1]Astromat. Sci. Res. Group, Inst. Space Astronaut. Sci., Japan Aerosp. Explor. Agnecy, 3-1-1 Yoshinodai, Chuo, Sagamihara, Kanagawa 252-5210, Japan (yada@planeta.sci.isas.jaxa.jp), [2] Marine Works Japan Ltd., 3-54-1 Oppamahigashi, Yokosuka 237-0063 Japan, [3]Dept. Earth Planet. Sci., Grad. Sch. Science, Univ. Tokyo, 7-3-1 Hongo, Bunkyo, Tokyo 113-0033, Japan, [4]Dept. Earth Science, Grad. Sch. Science, Hokkaido Univ., Kita 8, Nishi 5, Kita, Sapporo, Hokkaido 060-0808, Japan, [5]Earth-Life Sci. Inst., Tokyo Inst. Tech., 2-12-1-1E-1 Ookayama, Meguro, Tokyo 152-8550, Japan.

Introduction: The new era of sample return missions had started since the Stardust returned samples from comet 81P/Wild 2 in 2006 [1], followed by the Hayabusa spacecraft from the near-Earth S-type asteroid 25143 Itokawa in 2010 [2,3]. In this year, Hayabusa2 will reach its target body, the near-Earth C-type asteroid 162173 Ryugu [4], and also OSIRIS-REx toward the near-Earth B-type asteroid 101955 Bennu [5]. Additionally, several other sample return missions have been planned recently, such as the Martian Moons eXplorer (MMX) for the Phobos and/or Deimos [6], the CAESAR for 67P/Churyumov-Gerasimenko [7], and the HELACLES for the the Moon [8]. Therefore, returned-sample curation is increasing its importance in those sample return missions, in order to maximize scientific gains of their missions. The Astromaterial Science Research Group (ASRG) of JAXA has been managing curatorial works of Hayabusa-returned samples since its return in 2010, and preparing for sample curation of Hayabusa2 samples, which is planned to be returned in 2020.

Present status of curatorial works for Hayabusa-returned samples: Major advantages of the returned samples by missions compared with meteorites and cosmic dust found on the Earth are contamination control against the terrestrial environment and identification of their sampling bodies and positions. In order to keep these advantages of Hayabusa-returned samples, the ASRG developed the clean chambers in ultra-pure nitrogen or ultra-high vacuum conditions not to expose samples to the terrestrial atmosphere and contaminate them with the terrestrial detritus grains. They are installed in a cleanroom of class better than 1,000 in Fed. Std. 209E [3]. Environments of both the cleanroom and clean chambers have been monitored periodically by silicon wafers exposure method assisted by chemical analyses with a thermal decomposition GC-MS and a vapor-phase decomposition ICP-MS [9]. We installed an electrostatically controlled micro-manipulator in the clean chamber, which have been used for handling particles of 10-300μm in size, recovered from the sample container returned by Hayabusa. Additionally, the particles have been transfer to the FE-SEM/EDS for initial description using a sealable sample holder without exposing to air. Then they have been given their own ID numbers and listed on the database, which is open in public on the website of the ASRG (https://curation.isas.jaxa.jp/curation/hayabusa/index.html). More than 700 particles have been given IDs so far, and most of them are available for the international announcement of opportunity of research, which had started since 2012 and is still going on. We plan to finish initial descriptions of whole the Hayabusa-returned samples until 2020.

Preparation status of curation for Hayabusa2-returned samples: In parallel with the curatorial works mentioned above, the ASRG has developed clean chambers for Hayabusa2-returned samples in cooperation with advisory committee of specification of curation facility for Hayabusa2-returned samples. A new cleanroom of class 1,000 had been established in last summer, in where new clean chambers for Hayabusa2-returned samples will be handled. The new clean chambers (CCs) are basically composed of five components; CC3-1, 3-2, 3-3, 4-1, and 4-2, the former three for vacuum processes and the latter two for those in purified nitrogen conditions. We plan to unclose the sample container of Hayabusa2 and extract the sample catcher in the CC3-1, then transfer to the CC3-2 to unclose the catcher and obtain some fraction of the samples inside the catcher in vacuum. Then the catcher will be transferred to the CC3-3 to be purged in purified nitrogen condition and further sent to CC4-1 and 4-2 to be observed by an optical microscope, weighed by a balance, and the samples in there to be extracted for further descriptions. The final parts of CCs (CC3-3, 4-1, and 4-2) are now under installation. Then the ASRG will start their functional checks after their installations, followed by a series of rehearsals for initial processes of the returned samples, which will continue until the Hayabusa2 sample return in 2020, in cooperation with the sampler team and the initial analyses team of the Hayabusa2 mission.

References: [1] Brownlee D. et al. (2006) *Science* 314, 1711. [2] Abe M. et al. (2011) *LPS XLII*, Abstract #1638. [3] Yada T. et al. (2014). *Meteoritics & Planetary Science* 49, 135. [4] Watanabe S. et al. (2017) *Space Sci. Rev.* 208, 3. [5] Lauretta D. et al. (2017) *Space. Sci. Rev.* 212, 925. [6] Fujimoto M. et al. (2017) *EPSC2017*, Abstract #136. [7] Squyres S. W. et al. (2018) *LPS XLIX*, Abstract #1332. [8] Karouji Y. et al. (2018) *New Views of the Moon 2 – Asia*, Abstract #6053. [9] Karouji Y. et al. (2014) *Chikyukagaku (Geochemistry)* 48, 211.

PHYSICAL PROPERTIES OF SILICATE-RICH REGOLITH PARTICLES FROM ITOKAWA ASTEROID

S. Tanbakouei[1,2], J.M. Trigo-Rodríguez[1,2], and J. Sort[3,4]

[1]*Institute of Space Sciences (ICE-CSIC), Campus UAB, Carrer de Can Magrans s/n, 08193 bellaterra(Barcelona), Catalonia, Spain,*

[2]*Institut d'Estudis Espacials de Catalunya (IEEC), C/ Gran Capità, 2-4, Ed. Nexus, desp. 201, 08034 Barcelona, Catalonia, Spain,*

[3]*Departament de Física, Universitat Autònoma de Barcelona, E-08193 Bellaterra, Spain,*

[4]*Institució Catalana de Recerca i Estudis Avançats, Passeig Lluís Companys 23, E-08010 Barcelona, Spain.*

Introduction: The Hayabusa spacecraft rendez-voused with asteroid 25143 Itokawa in 2005 and brought regolith samples, collected during two touchdowns carried out on 19 and 25 November 2005 in its smooth terrain (MUSES-C), and returned to Earth in a sample-return capsule in 2010 [1]. The Itokawa reflectance spectrum corresponds to that of S-type asteroids, and its bulk mineralogy is consistent with the LL group of ordinary chondrites [2]. The surface of Itokawa consists of non-uniformly distributed boulders and regolith [3]. Cratering structures on Itokawa of meter- to hundred-meter sizes have been identified [3]. Evidence of a re-arrangement of boulders and migration of regolith, possibly owing to impact or tidal shaking, has also been identified on Itokawa [3-4]. Here we concentrate in studying the mechanical and magnetic properties of three regolith particles returned by Hayabusa mission using the nano-indentation technique. Our methodology, first applied to meteorites in a previous work [5], could be used in a next future to study the properties of Ryugu materials to be returned by Hayabusa 2.

Technical Procedure: Three Itokawa particles provided by JAXA, embedded in epoxy resine and polished to mirror-like appearance, with numbers RA-QD02-0014, RA-QD02-0023 and RA-QD02-0047 (hereafter designated as S14, S23 and S47 for simplicity) were investigated. First three samples were analyzed by optical microscopy and scanning electron microscopy (SEM). A scanning electron microscope FEI Quanta 650 FEG is working in a low-vacuum BSED mode. An EDX Inca 250 SSD XMax20 detector with an active area of 20 mm^2 is applied for elemental analysis of the samples. Micro-Raman spectra with a spot size of approximately 1 μm and laser power below 0.6 mW were obtained in order to study the shock experienced by the samples and give us chemical and structural information of different phases. Backscatter measurements were done at room temperature using the 5145 Å line of an Argon-ion laser with a Jobin-Yvon T-64000 Raman spectrometer attached to an Olympus microscope which equipped with a liquid nitrogen–cooled CCD detector. The Raman spectrometer is working in windows between 100 and 1400 cm^{-1} to acquire high resolution spectra.

The mechanical properties (hardness and reduced Young's modulus) were evaluated by the method that Oliver and Pharr (1992) first used. We choose the maximum applied forces of 5 mN and 10 mN in order to keep the maximum penetration depth below one fifth of the overall thickness of the sample. We applied some necessary corrections for the contact region and adoption of the instrument. We also kept the thermal drift below 0.05 nm·s^{-1}. The contact stiffness, was defined as:

$$S = dP/dh \qquad (1)$$

P denotes the applied load and h means the penetration depth during nanoindentation. P_{max} is the maximum load applied in the surface area A. Hence Hardness was calculated from the following equation:

$$S = \frac{P_{max}}{A} \qquad (2)$$

The elastic recovery calculated as the ratio between the elastic energy, U_{el} -estimated from the area between the unloading indentation segment and the x-axis- and U_{tot} (U_{el}+U_{pl}, where U_{pl} is the plastic energy)- estimated as the area between the loading indentation segment and the x-axis.

We also determined the reduced Young's modulus, E_r, defined as:

$$\frac{1}{E_r} = \frac{1-\nu^2}{E} + \frac{1-\nu_i^2}{E_i} \qquad (3)$$

The elastic displacements occur in all three samples, with Young's modulus E and Poisson's ratio ν, and the indenter, with elastic constants E_i and ν_i. Representative nanoindentation curves for one of the studied particles are shown in Fig. 1, from which the mean mechanical properties resulted from the analyzed region, can be extracted (Table 1).

As the hardness values are not remarkably different at 5 and 10 mN, it seems that the hardness has not affected by amount of the indentation load. It means that with our chosen loads, the strain-hardening phenomena that could happen due to the indentation size effect was avoided.

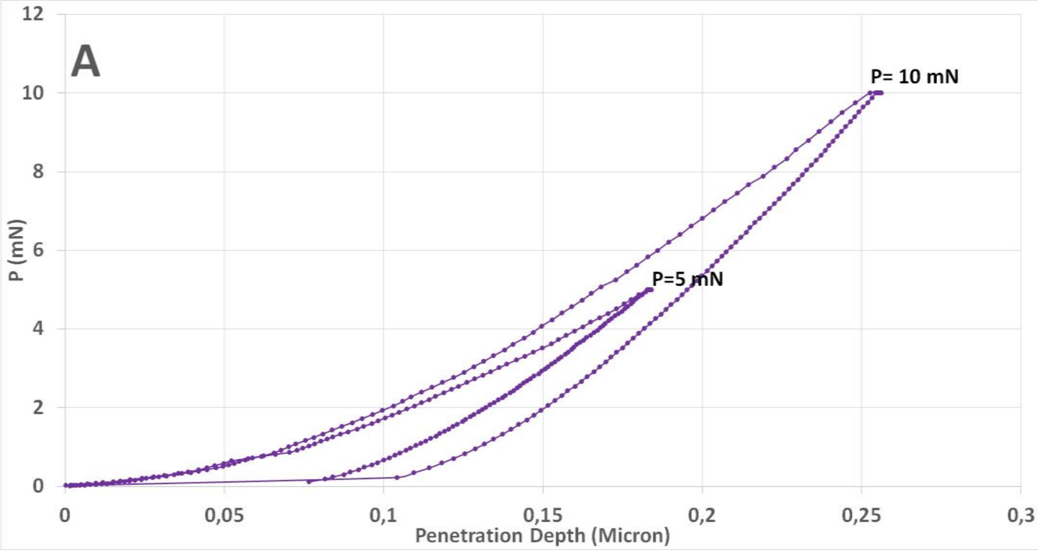

Figure 1. Indentation curve obtained for S14 sample.

Table 1. Average mechanical properties for three silicate-rich regolith particles of asteroid Itokawa. Reduced Young's modulus (E_r), hardness (H), constant stiffness (S), elastic recovery (U_{el}/U_{tot}) and plasticity index (U_{pl}/U_{tot}) were calculated by averaging the results from two lines of indentations from the maximum applied force of 5 mN.

E_r (GPa)	H (GPa)	S (mN/ micron)	U_{el}/ U_{tot}	U_{pl}/ U_{tot}
93.0 ± 0.20	10.33 ± 0.03	77.0 ± 0.20	0.75 ± 0.07	0.25 ± 0.07

Conclusions: Itokawa regolith is made of fractured particles produced by the collisional gardening of its surface along the eons. Their forming silicates are shocked, annealed and chemically homogenized, as we have also demonstrated using Raman spectroscopy [4]. This is consistent with regolith particles created by disaggregation, primarily as a response to impacts, but thermal fatigue cannot be ruled out in some cases [5]. In general, the mechanical properties of Itokawa regolith particles are comparable with silicates forming LL chondrites like e.g. Chelyabinsk. In any case, the elastic recovery of Chelyabinsk meteorite minerals exhibit lower values than these measured for Itokawa regolith grains. Despite of the homogeneous composition, we have discovered that some particles have distinctive areas that have been preferentially shocked. The induced drift in the positions of the olivine Raman peaks is due to changes in the olivine structure, typically associated with a structural rearrangement of the lattice. On the other hand, the reduced Young's modulus values obtained here for the Itokawa meteorite are above the measured for Chelyabinsk meteorite [6]. There is difference in the Young's modulus but hardness values are similar. Concerning the magnetic properties, we have found a soft magnetic behavior with a coercivity of around 70 Oe. The observed magnetic properties are consistent with the presence of tiny Fe and Ni inclusions in the samples, as was detected by energy-dispersive X-ray (EDX) analyses, leading to the formation of FeNi, FeO or FeS_2, among others.

Acknowledgements: This study was supported by the Spanish grant AYA 2015-67175-P, and ST made this study in the frame of a PhD. on Physics at the Autonomous University of Barcelona (UAB). We also thank Dr. Toru Yada and the Hayabusa curation staff of JAXA for providing the samples analyzed here.

References

[1] Yano et al. (2006) Science 312, 1350–1353. [2] Abe M. et al. (2006) Science 312, 1334–1338. [3] Saito J. et al. (2006) Science 312, 1341–1344. [4] Tanbakouei S. et al. (2018) submitted [5] Matsumoto et al. (2016) GCA 187, 195–217. [6] Moyano-Cambero C.E. et al. (2017) ApJ 835:157, 9 pp.

Establishing Itokawa's water contribution to Earth

Ziliang Jin[1] and Maitrayee Bose[1]
[1] *Center for Isotope Analysis, School of Earth and Space Exploration, Arizona State University, Tempe, AZ 85287.*

Japan's Hayabusa mission returned with more than 1500 particles from the S-type asteroid 25143 Itokawa and provided us with a plethora of information on small (≤20 km) undifferentiated bodies. Different from C-type asteroids, S-type asteroids are supposed to have originated in the inner solar system [1]; and we asked the question: Could Earth have acquired its volatiles from S-type asteroid bodies like Itokawa? Water, as we know, is critical to the formation of terrestrial planets and the origin of life. Most of the inner solar system objects contain at least 200 ppm water [2-4]. Earth is unique and contains abundant liquid water with 330–1200 ppm in its primitive mantle [4]. The origin of water on Earth is highly debated. To shed light on this issue, we measured water contents and D/H ratios in low-calcium pyroxenes (LPx) from Itokawa collected from Muses sea.

The water concentrations of two Itokawa grains are 700 ± 50 ppm (2σ) and 988 ± 50 ppm (2σ). These numbers have been corrected for galactic-cosmic-ray spallation events based on the reported 8 Ma exposure age of Itokawa [5], and the H and D production rates [6, 7]. We developed a thermal-diffusion model based on the one-dimensional Fick's law to correct for water-loss events, namely thermal metamorphism and impacts [8]. Based on the mineral proportions in Itokawa (67.2 wt.% olivine, 18.1 wt.% LPx and 2.6 wt.% high calcium pyroxene) [9], the estimated water content of Bulk Silicate Itokawa (BSI) ranges from 330 to 1570 ppm. The δD values of the Itokawa LPx grains after galactic-cosmic-rays spallation correction are -61 ± 16 ‰ (2σ) for RA-QD02-0057 and -35 ± 12 ‰ (2σ) for RA-QD02-0061. The Itokawa D/H ratio is indistinguishable from those of terrestrial and lunar samples, ordinary chondrites, carbonaceous chondrites, and meteorites from Vesta and Mars. Therefore, based on the estimated BSI water contents and δD values of Itokawa, we infer that the original planetesimals, e.g. S-type asteroids, in inner solar system are hydrous and could be a potential contributor to the total water budget of Earth or inner solar system bodies.

We will present the H isotope data on Itokawa particles and LL6 LAR12036 and LL5 LAR12241 ordinary chondrites, introduce our new thermal diffusion model, and discuss the implications of these results at the meeting.

References

[1] Walsh K. J. et al. 2011. Nature 475: 206. [2] McCubbin F. M. et al. 2012. Geology 40: 683. [3] Hauri E. H. et al. 2015. Earth and Planetary Science Letters 409: 252. [4] Peslier A. H. et al. 2017. Space Science Reviews 212: 743. [5] Nagao K. et al. 2011. Science 333: 1128. [6] Füri E. et al. 2017. Earth and Planetary Science Letters 474: 76. [7] Merlivat L. et al. 1976. Lunar and Planetary Science Conference Proceedings 7: 649. [8] Ingrin J. and Blanchard M. 2006. Reviews in Mineralogy and Geochemistry 62(1): 291. [9] Tsuchiyama A. 2014. Elements 10 (1):45.

The origin of hydrogen in space weathered rims of Itokawa regolith particles.

L. Daly[1] M. R. Lee[1], L. J. Hallis[1], P. A. Bland[2], S. M. Reddy[2,3], D. W. Saxey[3], W. D. A. Rickard[3], D. Fougerouse[2,3], N. E. Timms[2], F. Jourdan[2], M. A. Cox[2], T. Salge[4], H.A. Ishii[5], J.P. Bradley[5], J.Aguiar[6], K. Hattar[7], L.P. Keller[8], M.S. Thompson[8], R. Christoffersen[8]

[1]School of Geographical and Earth Sciences, University of Glasgow, Glasgow, G12 8QQ, UK. (luke.daly@glasgow.ac.uk).
[2]Department Earth and Planetary Science, Curtin University, GPO Box U1987, Perth, WA 6102, Australia.
[3]Geoscience Atom Probe Facility, Advanced Resource Characterisation Facility, John de Laeter Centre, Curtin University, GPO Box U1987, Perth, WA 6845, Australia.
[4]Imaging and Analysis Centre, Natural History Museum, Cromwell Road, London, SW7 5BD, UK.
[5]Hawaii Institute of Geophysics and Planetology, University of Hawaii at Manoa, Honolulu, HI, 96822.
[6]Idaho National lab, Idaho Falls, Idaho, USA.
[7]Sandia National Laboratories, PO Box 5800, Albuquerque, New Mexico, 87185, USA.
[8]Robert M Walker Laboratory for Space Science, Code KR, Astromaterials Research and Exploration Science, NASA Johnson Space Center, Houston, TX, 77058, USA.

Introduction: Space weathering is the combined action of the solar wind, solar flares, micrometeorite impacts, and galactic cosmic rays [1]. These processes alter the physical and chemical properties of surfaces exposed to the vacuum of space. Within Itokawa particles, space weathering features include 20-40 nm thick amorphous and vesiculated rims and Fe nanoparticles ($_{np}$) [2, 3], as well as ~100-300 nm diameter micrometeorite impact craters [4]. Space weathering also implants elements contained within the solar wind, in particular the noble gases, He and Ne [5], as well as H [6]. Hydrogen is particularly important as it may react with Itokawa silicates to produce OH and H_2O; OH has been observed in space weathered rims of interplanetary dust particles [6]. The possibility of generating water through the interaction of solar wind with silicate minerals may have significant implications for the origin of water in the inner solar system. Therefore, it is important to quantify the abundance and distribution of these elements across these space weathering features, but also to ensure that such features are related to space weathering processes and not terrestrial contamination. Here we have combined field emission scanning electron microscopy (FE-SEM), transmission electron microscopy (TEM), time of flight secondary ion mass spectrometry (TOF-SIMS) and, for the first time, atom probe tomography (APT), to the study of space weathered rims in Itokawa regolith particles. For comparison, analyses were performed on San Carlos olivine reference materials that had been irradiated with low energy He or deuterium (D).

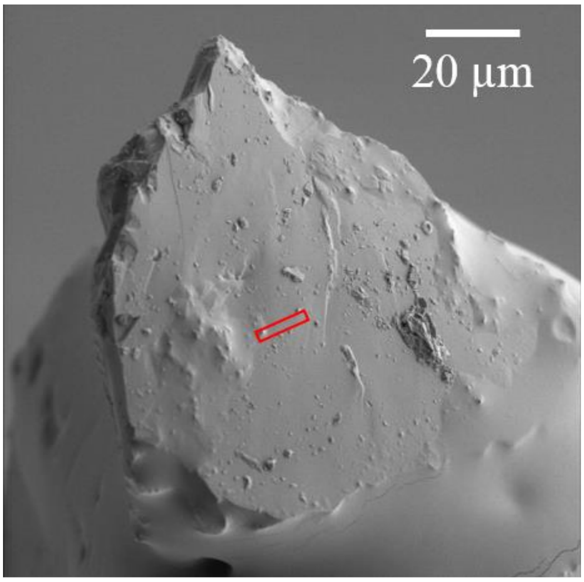

Figure 1: SE image Itokawa particle RA-QD02-0293. Atom probe specimens were extracted from the red box

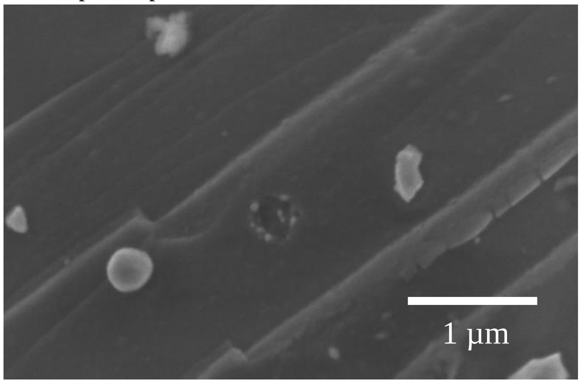

Figure 2: A SE image of a micrometeorite impact crater in Itokawa particle RA-QD02-0278.

Methods: Itokawa particle RA-QD02_0279 was mounted on a glass rod (Figure 1) and particles RA-QD02_0278 and RB-CV-0087 were mounted on carbon tape. RA-QD02_0278 and RB-CV-0087 were initially characterised at the Natural History Museum to identify mineral phases and space weathering features such as micrometeorite impact craters (Figure 2) using an FEI Quanta 650 FE-SEM with an annular Bruker energy dispersive X-ray spectrometer (EDS) inserted between the pole piece and the sample. This geometry allows non-destructive analysis at sub-micron resolution of uncoated samples with substantial surface topography by using ultra low beam current (25 pA) and low accelerating voltage (6kV) under high vacuum. The particles were then sputter coated with 200 nm of Cr to protect the sample from FIB-SEM sample preparation. Using a TESCAN LYRA3 FIB-SEM at Curtin University, APT needles were extracted by focussed ion beam (FIB) techniques [7], and TOF-SIMS ion maps were acquired from RA-QD02_0279 using both a negative and positive ion beam. The resulting 100 nm diameter APT needles were analysed at the geoscience atom probe facility (Cameca LEAP 4000X HR) at Curtin

University. Electron-transparent foils were also extracted from regions of the particles adjacent to the atom probe needles for correlative high resolution TEM and EDS. APT needles were also extracted from San Carlos olivine, both from pristine grains and from samples that had been implanted with He and D using a 10 kV Colutron accelerator.

Results and discussion: SEM imaging indicates that particle RA-QD02_0278 has several circular features on its surface that we interpret as micrometeorite impact structures (Figure 2), whereas RA-QD02_0279 and RB-CV-0087 lack such structures (Figure 1). EDS maps collected from the circular features in RA-QD02_0278 indicate that they have a similar chemical composition to the host olivine grain and so are likely to have been formed by secondary impact ejecta. Four APT datasets, each containing over 50 million ions, were collected from RA-QD02_0279 and one APT data set through a micrometeorite impact crater was collected from RA_QD02_0278. In all APT datasets evaporation commenced in the Cr coating, giving confidence that the outermost surfaces of the particles were measured, which have been potentially altered by space weathering features. The bulk chemistry derived from the APT data from RA-QD02_0279 indicate it is olivine (Fa_{30}). He and Ne were not observed in the mass spectrum and no Fe_{np} were detected. However, nanoscale domains of heterogeneous densities were observed in the outermost 20-30 nm (Figure 3). The high-density regions are enriched in Mg. Three of the four RA-QD02_0279 APT datasets show an enrichment of up to ~1.2 at. % in OH and H_2O ions that extends inwards for ~50 nm from the outer surface of the olivine particle. None of these features were observed in the pristine San Carlos olivine. TEM measurements of Itokawa, and APT data collection from the irradiated San Carlos olivine reference materials are ongoing and these results along with the implications of these new atomic scale observations will be presented at the meeting.

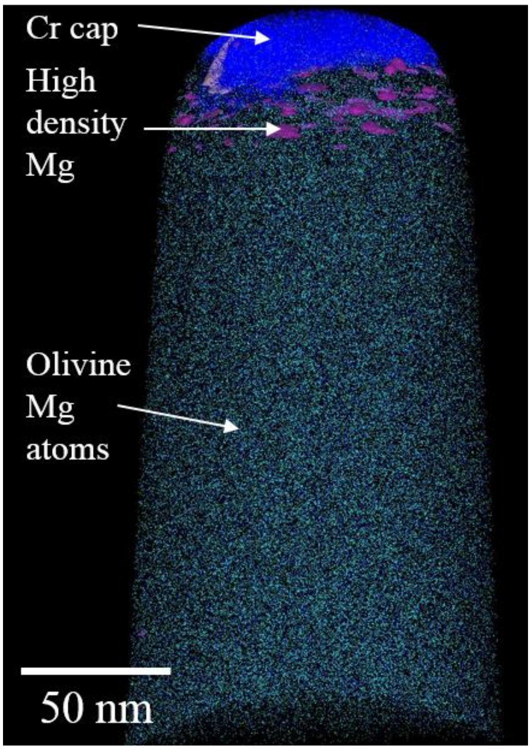

Figure 3: Atom probe needle of a space weathered rim of Itokawa. The blue and teal dots represent individual atoms of Cr and Mg, respectively. The protective Cr cap is clearly visible where the blue atoms are concentrated at the top of the needle. Pink isosurfaces depict Mg-rich, high-density regions close to the surface of the olivine grain.

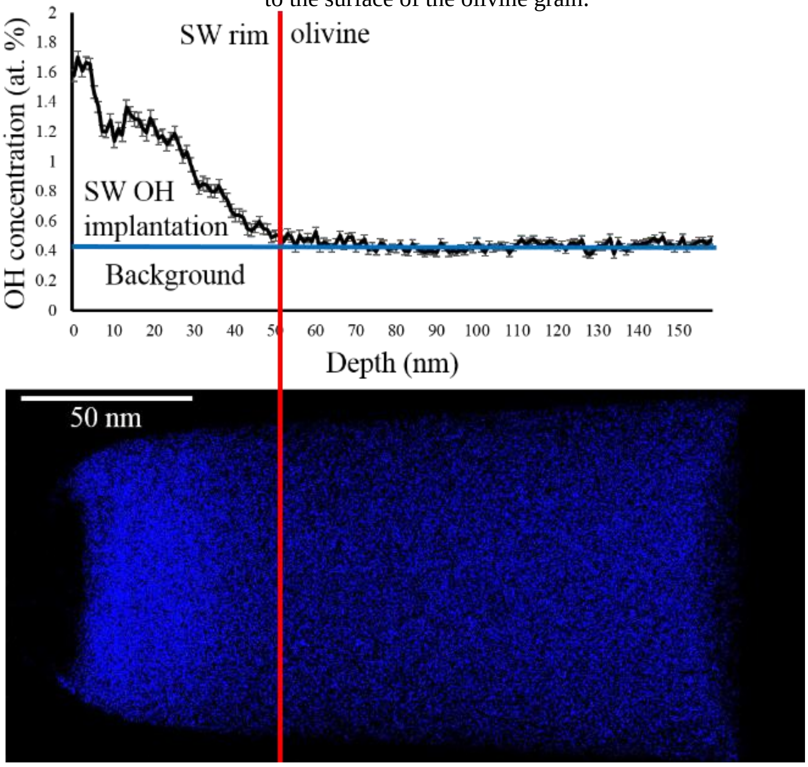

Figure 4: Atom probe needle of a space weathered rim of Itokawa. The blue dots represent OH ions, which are enriched up to 1.2 at. % in the outer 50 nm of the particle (left hand side).

References:

[1] Chapman C.R., (2004) *Ann. Rev. of Earth & Planet. Sci.,* 32, 539-567. [2] Noguchi T., et al., (2011), *Science,* 333, 6046, 1121-1125. [3] Noguchi T. et al., (2014) *MAPS*, 49, 2, 188-214. [4] Harries D., et al., (2016), *EPSL*, 450, 337-345. [5] Nagao K., et al., (2011) *Science,* 333, 6046, 1128-1131. [6] Bradley J.P., et al., (2014) *PNAS,* 111, 5, 1732-1735. [7] Thompson K., et al., (2007), *Ultramic.*, 107(2), 131-139.

Acknowledgements: This work is funded by UKSTFC and a UAE seed grant. This work was performed, in part, at the Center for Integrated Nanotechnologies, an Office of Science User Facility operated for the U.S. Department of Energy (DOE) Office of Science. Sandia National Laboratories is a multi-mission laboratory managed and operated by National Technology and Engineering Solutions of Sandia, LLC., a wholly owned subsidiary of Honeywell International, Inc., for the U.S. DOE's National Nuclear Security Administration under contract DE-NA-0003525. The views expressed in the article do not necessarily represent the views of the U.S. DOE or the United States Government.

Synchrotron Nanoprobe Analysis of Space Weathered Itokawa Grains

L. J. Hicks[1], J. C. Bridges[1], T. Noguchi[2], T. Ireland[3], A. Miyake[4], and J. D. Piercy[1]
[1]*University of Leicester, UK* (ljh47@le.ac.uk)
[2]*Kyushu University, Japan*; [3]*Australian National University, Australia*; [4]*Kyoto University, Japan*

Space weathering on Itokawa is largely the result of the bombardment by electrons and protons from the Solar Wind. Its effects are manifested by darkening and reddening of the affected surfaces [1]. In order to make the most detailed and accurate mineralogical analyses possible of space weathering effects in grains of Asteroid Itokawa, returned by the *Hayabusa* mission, we perform a multi technique characterisation of their mineralogy and isotopes at the sub-micron scale.

Five Itokawa grains allocated to this study are RB-QD04-0063, RB-QD04-0080, RB-CV-0089, RB-CV-0011, RB-CV-0148. Each were embedded in epoxy resin and ultramicrotomed for ultra-thin (~100 nm) sections which were observed using a JEOL JEM-ARM200F at the Ultramicroscopy Research Center, Kyushu University. The original potted butts were embedded again in epoxy resin to prepare polished samples 8 mm in diameter for SHRIMP analysis by using Leica EM TXP. From these embedded grains, FIB-SEM sections were obtained for TEM analyses and X-ray synchrotron nanoprobe analyses.

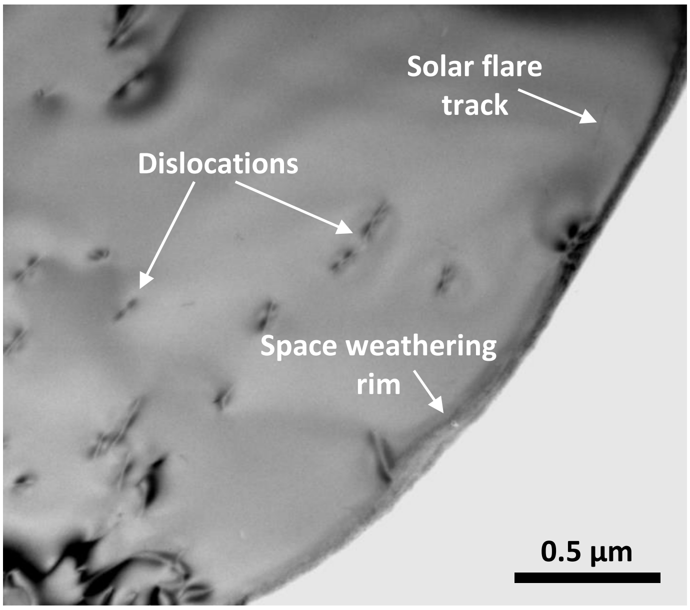

Figure 1. Bright-Field TEM image of RB-CV-0089, a low-Ca pyroxene grain featuring a <1 µm thick space weathering rim.

TEM-EDS chemical composition measurements have been performed on the FIB sections using a JEOL JEM-3200 FSK. Four of the five Itokawa grains are olivines, whereas RB-CV-0089 (shown in Figure 1) is a low-Ca pyroxene featuring high-Ca pyroxene inclusions. RB-QD04-0063 olivine grain also features plagioclase inclusions. All of the FIB sections have space weathering rims.

X-ray synchrotron analyses will be performed using the I-14 nanoprobe Beamline at *Diamond Light Source*, UK. The I-14 Beamline is capable of measuring a wide energy range (5-23 keV) down to a spatial resolution of 50 nm, and raster scanning to produce XRF/XANES mapping. Based on Fe-K X-ray Absorption Spectroscopy (XAS), we obtain high resolution XRF/XANES maps, XAS spectra, and ptchography imaging, analysing the five Itokawa grains in detail, with particular emphasis in the Fe redox changes and associated textures of space weathering. A typical Fe-K XAS measurement, for analysing the Fe redox, ranges from 7000 to 7300 eV with a higher resolution range of energy increments over the XANES features (~7100-7150 eV). The raw XAS and XANES data is then processed using *Athena 0.8.056* and *DAWN 1.9* [2]. Analysing the shifts in the Fe-K absorption edge and $1s \rightarrow 3d$ pre-edge peak centroid, and comparing to ferromagnesian silicate reference materials of known ferric-ferrous content, it is possible to semi-quantitatively deduce the oxidation state of our samples, similarly to previous studies of Itokawa, Comet Wild 2, and martian meteorite samples [3,4,5,6]. The high spatial resolution of I-14 will allow us to map the variation in Fe oxidation state across Itokawa grains and relate this to metallization associated with potential space weathering in the grains.

This X-ray nanoprobe analysis of Itokawa samples will reveal new insights into the redox changes associated with space weathering, informing further studies of other airless Solar System bodies such as the returned samples of asteroids Ryugu and Bennu from the *Hayabusa 2* and *OSIRIS-REx* missions.

References

[1] Binzel R. P. et al. 2001. Meteoritics & Planetary Science, 36, 1167-1172. [2] Basham M. et al. 2015. Journal of Synchrotron Radiation, 22, 853–858. [3] Noguchi T. et al. 2014. Earth, Planets and Space, 66, 124-133. [4] Hicks L.J. et al. 2017. Meteoritics & Planetary Science, 52, 2075-2096. [5] Changela H. G. 2012. Geochimica et Cosmochimica Acta, 98, 282-294. [6] Hicks L.J. et al. 2014. Geochimica et Cosmochimica Acta, 136, 194-210.

Collisional fragmentation of an olivine-enstatite-rich Itokawa particle

Agnese Fazio[1], Dennis Harries[1] and Falko Langenhorst[1,2]
[1]*Analytical Mineralogy of Nano- and Microstructures, Institute of Geosciences, Friedrich Schiller University Jena, Germany*
[2]*Hawai'i Institute of Geophysics and Planetology, School of Ocean and Earth Science and Technology, University of Hawai'i at Manoa, USA (Falko.Langenhorst@uni-jena.de)*

Introduction: The regolith grains sampled and returned to Earth by the spacecraft Hayabusa from asteroid 25143 Itokawa allowed for the second time – after the Apollo missions – the direct study of space weathering effects [1] and confirmed the link between ordinary chondrites and the S-type asteroid [2]. The reported space weathering effects are due to both solar wind irradiation and impacts of micrometeoroids. They include nanocrystalline and amorphous layers [2-6], melt- and vapor-deposited layers [3, 5], and shock metamorphic features (e.g., lattice defects) [7]. In this work, we present the results of a study on grain RB-QD04-0092. This particle documents the complex dynamic evolution of the asteroid surface by impact gardening.

Sample and methods: In the context of the 4th International Announcement of Opportunity for Hayabusa sample investigation, we have received five Itokawa particles. Currently, we have focused on the investigation of particle RB-QD04-0092, which was sliced into five subsamples by focused ion beam (FIB) on a scanning electron microscope (SEM) and then studied by analytical transmission electron microscopy (TEM), following the procedure described by [6].

Observations and discussion: RB-QD04-0092 is a flat grain (29 x 25 x 8 µm) consisting of enstatite (En75-80) and olivine (Fo71-78). Numerous mineral fragments are attached to its surface (Fig. 1). They are mainly made of Mg-rich olivine, troilite, and plagioclase.

TEM reveals that the entire particle possesses a polycrystalline rim (maximum thickness 70 nm) and incipient vesicle/blister formation, indicating a moderate solar wind exposure [8]. Contrary to other observations [2], no (sulfur)-iron nanoparticles and amorphized rims were found. Solar flare tracks were observed in both enstatite and olivine with a density comparable to previously reported data (10^8 – 10^9 cm^{-2}; [4, 6]).

In addition to these features, olivine and enstatite show typical shock effects known for shocked meteorites, that is: (1) screw dislocations with Burgers vector [001] in olivine and (2) (100) clinoenstatite lamellae in orthoenstatite. This is the first report of clinoenstatite lamellae in Hayabusa-returned samples. Dislocations in olivine occur localized in at least three separate sites, suggesting more than just one impact event. We found a maximum length of the [001] dislocations of 2.5-3 µm. Taking the estimated dislocation velocity in experimentally shocked olivine [9], their time of propagation and, hence, shock duration can be approximated to be of the order of 1.5 ns. This short time indicates that the multiple collisions that RB-QD04-0092 underwent must have occurred with other tiny particles or fragments in the regolith of Itokawa. Clinoenstatite lamellae are relatively short, which is also in agreement with such small-scale grain-grain collisions. However, impact microcraters are absent on the surfaces of sites with the aforementioned shock effects.

Conclusions: The absence of a well-developed amorphous rim containing nanoparticles and the occurrence of at least four sites with shock effects and no microcraters indicate that RB-QD04-0092 was involved in active regolith gardening. This collisional gardening has the effect of reducing the effective exposure time of regolith grains.

Acknowledgements
We are grateful to JAXA for providing Itokawa particles. FIB-TEM facilities at FSU Jena were funded by the Gottfried-Wilhelm-Leibniz award to FL (LA 830/14-1). AF thanks the Alexander von Humboldt Foundation for a postdoctoral grant.

References
[1] Bennett C.J., et al. 2013 Chemical Reviews 113:9086. [2] Noguchi T., et al. 2011 Science 333:1121. [3] Thompson M.S., et al. 2014 Earth Planets and Space 66:89. [4] Keller L.P. and Berger E.L. 2014 Earth Planets and Space 66:71. [5] Noguchi T., et al. 2014 Meteoritics & Planetary Science 49:188. [6] Harries D. and Langenhorst F. 2014 Earth Planets and Space 66:163. [7] Langenhorst F., et al. 2014 Earth Planets and Space 66:118. [8] Harries D., et al. 2018 Abstract #368. EPSC 2018. [9] Langenhorst F., et al. 1999 Earth and Planetary Science Letters 173:333.

Measuring Shock Stage of Itokawa and Other Asteroid Regolith Grains by Electron Back-Scattered Diffraction

Michael Zolensky[1], James Martinez[1], Scott Sitzman[2], Takashi Mikouchi[3], Kenji Hagiya[4], Kazumasa Ohsumi[5], Yasuko Terada[5], Naoto Yagi[5], Mutsumi Komatsu[6], Hikaru Ozawa[4], Yuta Taki[4], Yuta Yamatsuta[4], Atsushi Takenouchi[3], Hikari Hasegawa[3], Haruka Ono[3], Kotaro Higashi[3], Masaki Takata[5], Arashi Hirata[4], Ayaka Kurokawa[4], Shoki Yamaguchi[4].

[1]ARES, NASA JSC, Houston, TX (USA); [2]Aerospace Corporation, El Segundo, CA, (USA); [3]School of Science, Univ. of Tokyo (Japan); [4]Graduate School of Life Science, Univ. of Hyogo (Japan); [5]Japan Synchrotron Radiation Research Institute (Japan); [6]SOKENDAI (Japan).

Introduction: One of the fundamental aspects of any astromaterial is its shock history, since this factor elucidates critical historical events, and also because shock metamorphism can alter primary mineralogical and petrographic features, and reset sample chronologies [1-3]. Failure to take shock history into proper account during characterization can result in seriously incorrect conclusions being drawn regarding the formation and geological history of a body. Thus the Hayabusa Preliminary Examination Team (HASPET) made shock stage determination of the Itokawa samples a primary goal. However, we faced several difficulties in this particular research. The shock state of ordinary chondrite materials is generally determined by simple optical petrographic observation of standard thin sections, sometimes doubly polished but always of a uniform, set thickness. The Itokawa samples available to the analysis team were sometimes attached to carbon fibers, but more generally mounted into plastic blocks which were polished on only one side, and were of non-standard and greatly varying thickness, all of which significantly complicated petrographic analysis (but did not prevent it).

Shock State by EBSD: We made determination of the sample shock state of several Itokawa regolith grains by electron back-scattered diffraction (EBSD) [1-5]. Since EBSD is probably going to become the tool of choice for shock determination of regolith grains, we made a special effort to provide a solid foundation for this technique. Thus one goal of this work is to devise a bridge between shock determinations by standard light optical petrography, crystal structures as determined by electron and X-ray diffraction techniques [1-4]. We are comparing the Itokawa samples to L and LL chondrite meteorites chosen to span the shock scale experienced by Itokawa, specifically Chainpur (LL3.4, Shock Stage 1), Semarkona (LL3.00, S2), Kilabo (LL6, S3), NWA100 (L6, S4) and Chelyabinsk (LL5, S4). In this presentation we will concentrate on the EBSD work.

An important subtask of the EBSD work was to determine if shock state "standards" (meteorite samples of accepted shock state) show strain measurements that may be statistically differentiated, using a sampling of particles (number and size range) that may be expected from an asteroid sample-return mission. We are initially seeking "Indirect" evidence of impact shock since we are not seeking actual strain values, rather indirect strain-related measurements such as extent of intra-grain lattice rotation.

Our ultimate goal is to establish and then to apply the EBSD method, in particular, to regolith grains from near-earth asteroid Itokawa returned to Earth by the Hayabusa spacecraft, and ultimately add this capability to the planetary science took kit for subsequent missions and their resultant returned astromaterial particles.

Our research will improve our understanding of how small, primitive solar system bodies formed and evolved, and improve understanding of the processes that determine the history and future of habitability of environments on other solar system bodies. The results will directly enrich the ongoing asteroid and comet exploration missions by NASA and JAXA, and broaden our understanding of the origin and evolution of small bodies in the early solar system, and elucidate the nature of asteroid and comet regolith.

Techniques: This work was begun under the auspices of the Hayabusa Sample Preliminary Examination Team (HASPET) activity, where many analyses were made in carefully planned sequential order, under very severe time constraints. One effect of the time constraint was that we frequently had only one opportunity to see a particular sample before it was partially or entirely consumed by a subsequent analysis. Since EBSD requires exceptionally well-polished samples we had to find a new procedure for the final polish. Rather than using water and colloidal silica, as is traditional for EBSD, we used a mixture of ethylene glycol, ethanol, glycerol, and 0.05 µm alumina, as recommended by George Vander Voort (personal communication, 2010). The resulting sample finish was slightly inferior to what could have been achieved using colloidal silica, but was adequate for our purposes.

We employed JSC's Supra 55 variable pressure FEG-SEM and Bruker EBSD system. We were not seeking actual strain values, but rather indirect strain-related measurements such as extent of intra-grain lattice rotation, and determining whether shock state "standards" (meteorite samples of accepted shock state, and appropriate small grain size) show strain measurements that may be statistically differentiated, using a sampling of particles (number and size range) typical of asteroid regoliths.

In order to usefully obtain and compare EBS patterns from astromaterial samples, we had to undergo a rather extensive optimization program for sample preparation and analysis settings. Unfortunately, we anticipate that each EBSD user must perform a similar procedure, especially for different SEM models. Using our system we determined that a column pressure of 9 Pa and no C-coating on the sample was optimal. We varied camera exposure time and gain to optimize mapping performance, concluding that 320x240 pattern pixilation, frame averaging of 3, 15 kV, and low extractor voltage yielded an acceptable balance of hit rate (>90%), speed (11 fps) and map quality using an exposure time of 30 ms (gain 650). We found that there was no strong effect of step size on Grain Orientation Spread (GOS) and Grain Reference Orientation Deviation angle (GROD-a) distribution; there was some effect on grain average Kernel Average Misorientation (KAM) (reduced with smaller step size for the same grain), as expected. We monitored GOS, Maximum Orientation Spread (MOS) and GROD-a differences between whole olivine grains and sub-sampled areas, and found that there were significant differences between the whole grain dataset and subsets, as well as between subsets, likely due to sampling-related "noise". Also, in general (and logically) whole grains exhibit greater degrees of cumulative lattice rotation. Sampling size affects the *apparent* strain character of the grain, at least as measured by GOS, MOS and GROD-a. There were differences in the distribution frequencies of GOS and MOS between shock stages, and in plots of MOS and GOS vs. grain diameter. These results are generally consistent with those reported by A. Ruzicka [5]. However, it is unknown whether the differences between samples of different shock states exceeds the clustering of these values to the extent that shock stage determinations can still be made with confidence. We are investigating this by examination of meteorites with higher shock stage 4 to 5.

Grain size vs. GOS/MOS distribution: We compared the grain size vs GOS and MOS distributions for Semarkona and Chelyabinsk, which have significantly different shock histories. Significant differences between plots of GOS and MOS vs grain size are apparent, and can be proposed as factors to be used to discriminate between different shock histories. It remains to be proven that these are due to differences in the inherent properties of these samples rather than due to differences in settings used for data acquisition, or to deconvolve these two and other potential sources. Notably, MOS shows considerably less difference in "illegal zone" limit position.

Conclusions: A major question we are addressing is: Do small fragments properly represent the strain state of larger rocks? And if so, how to measure that strain? Along these lines there are some important factors to consider. Subsets of larger grains generally don't fully represent the full range of strain behaviors exhibited by the largest grains in our EBSD maps by the strain-related measurements we're using (GOS, MOS, GROD-a, KAM and grain averaged KAM). There is not a 100%, completely clear relationship between grain size and GOS/MOS. However, a very preliminary comparison between Semarkona and Chelyabinsk indicated a significant strain difference, using GOS. Therefore, it appears that GOS can be used to reveal the impact shock histories of asteroidal samples, assuming that a sufficient number of samples or map areas are interrogated. Since there's no strong effect of grain size on some of the most important strain-related measures (e.g., GOS and GROD-a), perhaps small particles are may be reasonably characterized by relatively pixelated maps. Our results suggest that shock strain can be best elucidated by collection of especially slow, high quality EBSD maps (e.g., 640 x 480 camera binning, >1 frame averaging), even if they're only incrementally better than the standard balanced settings we used (320x240, 1 frame). The best results are obtained when completely comparable maps are collected. This means using identical (1) sample preparation techniques, (2) identical instrument and instrument conditions, (3) identical map settings, (4) similar mapping areas and/or number of grains. Since there are numerous SEM models being used by meteoriticists, it would be a best for a set of standard materials to be prepared and distributed in "round robin" fashion to all interested labs.

Acknowledgements: We thank JAXA for the Hayabusa samples. MEZ was supported by the NASA Hayabusa and Hayabusa2 Participating Scientist Programs.

References: [1] Zolensky et al. (2012) *Lunar and Planetary Science*, XLIII, #1477, Lunar Planet. Inst., Houston (CD-ROM); [2] Zolensky et al. (2014) *Hayabusa 2014: 2nd Symposium of Solar System Materials. Abstracts*.; [3] Zolensky et al. (2016) *Hayabusa 2016 Abstracts*; [4] Hagiya et al. (2016) *Abstracts, 79th Annual Meeting of the Meteoritical Society*; [5] Ruzicka and Hugo (2017) *80th Annual Meeting of the Meteoritical Society*, 6368.

U-Pb systematics of Hayabusa particles:
Constrains on the thermal and impact histories of 25143 Itokawa

K. Terada[1]*, Y. Sano[2], N. Takahata[2], A. Ishida[3], A. Tsuchiyama[4], T. Nakamura[3], T. Noguchi[5], Y. Karouji[6], M. Uesugi[7], T. Yada[6], M. Nakabayashi[1], K. Fukuda[8], H. Nagahara[8]

[1] *Graduate School of Science, Osaka University, Toyonaka 560-0043, Japan.*
[2] *Atmosphere and Ocean Research Institute, The University of Tokyo, Chiba 277-8564, Japan.*
[3] *Graduate School of Science, Tohoku University, Sendai 980-8578, Japan.*
[4] *Graduate School of Science, Kyoto University, Kyoto 606-8502, Japan.*
[5] *Faculty of Arts and Science, Kyushu University, Fukuoka 819-0395, Japan.*
[6] *JAXA, Sagamihara 252-5210, Japan.*
[7] *JASRI/SPring-8, Hyogo, 679-5198, Japan.*
[8] *Graduate School of Science, The University of Tokyo, Bunkyo-ku 113-0033, Japan.*

Understanding the origin and evolution of near-Earth asteroids (NEAs) is an issue of scientific interest and practical importance because NEAs are potentially hazardous to the Earth. However, when and how NEAs formed and their evolutionary history remain enigmas. Here, we report the U-Pb systematics of Itokawa particles for the first time. Ion microprobe analyses of seven phosphate grains from a single particle provide an isochron age of 4.64±0.18 billion years (1σ). This ancient phosphate age is thought to represent the thermal metamorphism of Itokawa's parent body, which is identical to that of typical LL chondrites [1]. In addition, the incorporation of other particles suggests that a significant shock event might have occurred 1.51±0.85 billion years ago (1σ), which is significantly different from the shock ages of 4.2 billion years of the majority of shocked LL chondrites [2] and similar to that of the Chelyabinsk meteorite [3]. Combining these data with recent Ar-Ar studies on particles from a different landing site [4], we conclude that a globally intense impact, possibly a catastrophic event, occurred ca. 1.4 Ga ago. This conclusion enables us to establish constraints on the timescale of asteroid disruption frequency, the validity of the crater chronology and the mean lifetime of small NEAs [5].

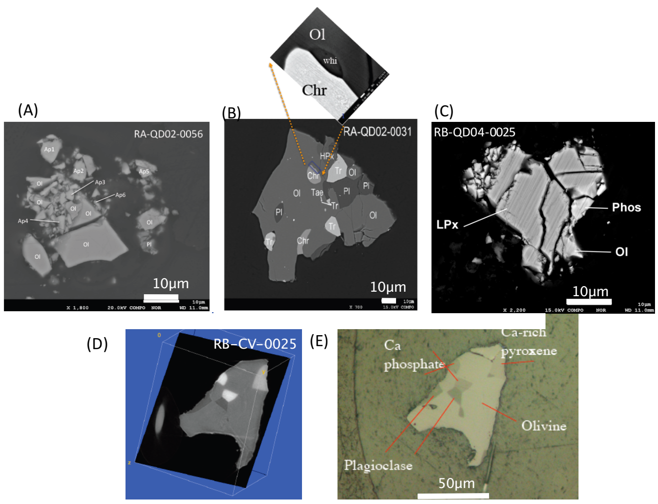

Figure 1. Cross sections of the Itokawa particles.

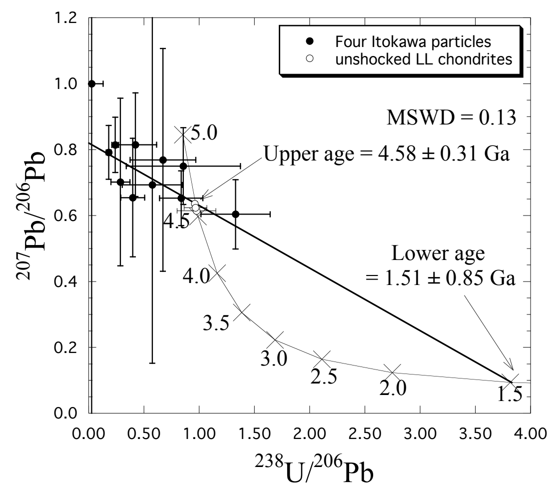

Figure 2. Tera-Wasserburg diagram of four Itokawa particles.

References

[1] Göpel C. et al. 1944. *Earth Planet. Sci. Lett.* **121**, 157-171.

[2] Swindle T. D. and Kring D. A. 2008. In: Workshop on Early Solar System Impact Bombardment, Lunar & Planetary Institute (abstract #3004).

[3] Righter K. et al. (2015) *Meteoritics & Planetary Science* **50**, 1790–1819.

[4] Park J. et al. 2015. *Meteoritics and Planetary Science* **50**, 2087-2098.

[5] Terada et al. 2018. Scientific Reports 8: 11806.

Itokawa, a >4.2 Ga old rubble pile asteroid

F. Jourdan[1], N.E. Timms[1], T. Nakamura[2], W.D.A. Rickard[1], E. Eroglu[1], C. Mayers[1], P.A. Bland[1], R. Oike[2] and T. Yada[3]

[1]*Curtin University, Perth, GPO Box U1987, WA, Australia*
[2]*Tohoku University, Aoba, Sendai, Miyagi 980-8578, Japan*
[3]*Institute of Space and Astronautical Science, JAXA, Sagamihara, Kanagawa 252-5210, Japan*

Asteroid 25143 Itokawa is a rubble pile asteroid consisting of reaccumulated fragments from a catastrophically disrupted monolithic parent asteroid, and from which regolith dust particles have been recovered by the Hayabusa space probe. When and how did the collision that resulted in the initial breakup of Itokawa's parent body occur? In a previous study [1], we obtained an age of 2291 ± 139 Ma on a single particle (#0013). Equilibration near the time of formation implies that this particle was formed deep inside the parent asteroid, yet a full reset of the K/Ar suggests that the particle was then close to the surface at 2.3 Ga. We then developed a novel temperature-pressure-porosity model, coupled with diffusion models to show that the relatively low pressure and high temperature involved in the impact process can be reconciled only if the asteroid was already made of porous material at ~2.3 Ga and thus, if asteroid Itokawa was already formed, thereby providing a *minimum* age for catastrophic asteroid breakup. In this study, we present SEM, EBSD, ToF-SIMS and $^{40}Ar/^{39}Ar$ dating results from four more particles (RA-QD02-0010, RA-QD02-0288, RB-CV-0082 and RB-QD04-1159). Unlike Particle #0013 [1], EBSD analyses show that none of these particles exhibit any noticeable sign of shock deformation, except perhaps one grain of troilite in particle #1159 which shows evidence of crystal-plastic deformation. Yet, $^{40}Ar/^{39}Ar$ analyses show the K/Ar system in all these particles has been reset at various ages.

<u>Particle #0288 and #1159</u> yielded two well-defined plateau ages of 4219 ± 35 Ma (P=0.58) and 4149 ± 41 Ma (P=0.27), respectively best interpreted as recording a high temperature, yet very low shock impact event. Considering that the parent planetesimal of Itokawa is unlikely to have had an internal source of heat for ~340 Ma after formation, the equilibrated particles must have been by then close to the surface to be exposed to any impact related thermal event. The very low level of shock indicated by EBSD analysis (<10 GPa) suggest a high porosity of 35-40 % to allow the particle to reach the level of post-shock temperature required to reset plagioclase (cf. models by Jourdan et al., [1]). This suggests that Itokawa (probably a larger version at the time) was already formed by 4.2 Ga, almost twice as long as previously estimated.

<u>Particle #0082</u> is a melt rock particle which petrography has been described by Nakamura et al. [2] and Timms et al. ([3]: this meeting). EBSD analysis shows no sign of shock in the pyroxene and olivine phenocrysts present amongst the glass. Unfortunately, $^{40}Ar/^{39}Ar$ analyses did not yield any resolvable plateau age but is consistent with recoil redistribution, an artifact caused by the neutron-activation of ^{39}Ar, thus suggesting an age of age of 4.4 – 4.5 Ga. Whereas initially considered as an impact melt rock, our preferred interpretation is currently that it is a fragment of a mesostasis-bearing porphyritic chondrule produced at the birth of the solar system (Timms et al., this meeting).

<u>Particle #0010</u> did not yield any plateau age but a single hump-shaped age spectrum. ToF-SIMS compositional analyses of the plagioclase revealed the presence of sub-micrometer-wide K-feldspsar exolution lamellae (antiperthite). An argon diffusion model suggests that a brief yet high temperature heating event at ~500 Ma is able to decouple the K-feldspar and plagioclase $^{40}Ar^*$ reservoirs and reproduce the observed single hump-shape spectrum.

Conclusions: Plagioclase-bearing equilibrated particles have recorded a series of impact events {~500 Ma, 1350 ± 250 Ma (multi-particles, [3]), 2291 ± 139 Ma [1], 4149 ± 41 Ma and 4219 ± 35 Ma} best interpreted as occurring at / or near the surface of Itokawa, which implies a larger version of the rubble pile was already formed by at least ~4.2 Ga. This suggests that rubble pile asteroids can survive ambient solar system bombardment for extremely long periods. Such a long-term survival makes sense considering that the "cushiony" rubble pile nature of an asteroid makes it more prone to absorb shock during impacts without further breaking apart due to a drastically reduced radius of the impact-induced shock zone in porous media.

References

[1] Jourdan et al., 2017. Geology 45. [2] Nakamura et al., 2017. Hayabusa symposium 2017. [3] Timms et al., 2018. Hayabusa symposium 2018. [4] Park et al., 2015. Meteoritics & Planetary Science 50.

Itokawa chondrule fragment preserves evidence of proto-planetary disk processing

N.E. Timms[1], F. Jourdan[1], W.D.A. Rickard[1], T. Nakamura[2], D.W. Saxey[1], D. Fougerouse[1], S.M. Reddy[1], L. Daly[3], P.A. Bland[1], Z. Quadir[1], R. Oike[2] and T. Yada[4]

[1]*Curtin University, Perth, GPO Box U1987, WA, Australia*

[3]*Tohoku University, Aoba, Sendai, Miyagi 980-8578, Japan*

[2]*University of Glasgow, Glasgow, G12 8QQ, UK*

[4]*Institute of Space and Astronautical Science, JAXA, Sagamihara, Kanagawa 252-5210, Japan*

(*correspondence: n.timms@curtin.edu.au)

Particles brought back from Itokawa provide a unique opportunity to study unaltered material in their original context (i.e. without glass hydration). Here we combine time of flight secondary ion mass spectrometry (ToF-SIMS), electron backscatter diffraction (EBSD), transmission electron microscopy (TEM), energy dispersive spectroscopy (EDS), $^{40}Ar/^{39}Ar$ geochronology, and Atom Probe Tomography (APT) to examine one of the few melt rock particles recovered from the Itokawa asteroid by the Hayabusa mission [1]. This particle (RB-CV-0082) comprises 5-30 μm long crystals of high-Ca Cr-bearing pyroxene, olivine within a quenched emulsion of variable composition silicate glass. The olivine (Fa = 26.7% via APT; 27.9% via EDS) is similar in composition to other olivine from equilibrated Itokawa particles. EBSD mapping reveals that the olivine and high-Ca pyroxene phenocrysts are crystalline and do not show any evidence of shock metamorphism or deformation. Furthermore, the high-Ca pyroxene form elongate clusters of grains that have a strong crystallographic and shape preferred orientation.

TEM imaging, EBSD and TOF-SIMS (≤50 nm spatial resolution) maps show two dominant glass compositions form interconnected globules, much of which is amorphous. These segregations are Si-Al-Na-K-O-rich and Ca-Fe-Mg-Ti-O-rich, and are plagioclase and pyroxene normative, respectively. Locally, nebulous segregations of Si-Al-Na-O-rich and crystalline Mg-Fe-Si-O-rich material are associated with partially- to totally-digested olivine grains. The glass also contains ~5%vol nano-vesicles (typically 10-300 nm across), and minor nano-scale crystals of troilite and merrillite. Within the Si-Al-Na-K-O-rich regions of the glass, the alkalis (including K relevant to $^{40}Ar/^{39}Ar$ dating) are further segregated into even finer lamellae, alternating over 100 nm length scales. Further nanoscale analyses by APT constrain the compositions of fine-scale domains within the particle, demonstrating that lamellae within Si-Al-Na-K-O domains comprise end-member orthoclase and albite normative compositions, consistent with antiperthite lamellae. The $^{40}Ar/^{39}Ar$ analysis of particle RB-CV-0082 indicates an approximate age of 4.5 Ga. However, the data show that the $^{40}Ar/^{39}Ar$ analysis is likely to be affected by recoil, precluding resolution of a precise age.

The texture of RB-CV-0082 is consistent with incipient flash melting, with complete digestion of feldspar and partial digestion of olivine and pyroxene. The various glass compositions are consistent with phase separation into conjugate immiscible liquids formed by spinodal decomposition upon cooling below the upper critical solution temperature in a multicomponent oxide system, preserved by rapid quenching [2]. Subsequent crystallization of the plagioclase-normative immiscible domains to plagioclase was followed by exsolution of Na and K- rich (antiperthite) lamellae upon cooling below the feldspar solvus.

It has been reported that the regolith from the Itokawa asteroid underwent long-term thermal annealing and subsequent impact shock [4]. It is possible that an impact event could have caused flash melting and quenching of a metamorphosed olivine-pyroxene-plagioclase parent rock responsible for the texture of this particle. This melting mechanism would help explain why the relict olivine composition is similar to that of normal Itokawa olivine while preserving interstitial fine-scale glass textures. However, the lack of shock microstructures in olivine and pyroxene grains, the crystallographic alignment of elongate (barred?) pyroxene, and extremely old $^{40}Ar/^{39}Ar$ age are more consistent with a porphyritic chondrule with mesostasis origin for the particle rather than an impact melt origin. As such, this particle provides more insight into chondrule formation within the proto-planetary disk than the history of the Itokawa parent body. Nevertheless, the preservation of such fine-scale microstructures and compositional variations in this particle imply that it has not been extensively texturally equilibrated via recrystallisation and grain growth at high temperatures associated with thermal metamorphism on the initial Itokawa parent body (as interpreted for the majority of the Itokawa particles). Therefore, this fragment was likely to have been sourced from near the surface of the Itokawa parent body prior to breakup. The preservation of nano-vesicles indicates that the timescales of flash heating and quenching were very short and did not result in the complete loss of volatiles, which has implications for volatile retention through chondrule formation and processing within the proto-planetary disk, as well as accretion, processing and breakup of the asteroid parent body.

References

[1] Nakamura. T. et al. 2014. Abstract at Hayabusa 2014. [2] Hamann et al. (2017). Meteoritics & Planetary Science 1-39. [3] Jourdan. F. et al. 2017. Geology 45:819-822. [4] Nakamura. T. et al. 2011. Science 333:6046.

Searching for Volatiles in Space Weathered Grains

Katherine D. Burgess[1] and Rhonda Stroud[1]
[1] *U.S. Naval Research Laboratory, Washington, DC, USA*

Space weathering alters the physical, chemical, and optical characteristics of materials on the surfaces of airless bodies. In our current understanding, solar wind ion irradiation and micrometeoroid bombardment, along with other processes, lead to the formation of thin amorphous coatings and nanophase metallic iron inclusions ($npFe^0$) that in turn are the main causes of darkening and reddening in the visible to near infrared wavelength region [1]. While we have been able to study lunar rocks and soils for the past almost 50 years and have gained an understanding of the main processes and effects of space weathering there, open questions about the rates at which alteration occurs and how various space weathering processes interact with each other remain. The return of samples from asteroid Itokawa has provided a new avenue for understanding the effects of space weathering and how the dominant processes can vary in different regions of the Solar System. Additionally, advances in scanning transmission electron microscopy (STEM) instrumentation and associated techniques have enabled new measurements and analyses of old and new samples and can provide new insights about space weathering processes and features [2,3].

Recent work on space weathered grains from the Moon and asteroid Itokawa have demonstrated that the phase of the substrate or host grain plays a significant role in how materials are altered by solar wind irradiation and micrometeoroid bombardment [2,4]. Vesicles and/or surface blisters are observed to be present in or on some phases but not others that are directly adjacent. The presence (or lack of) vesicles in some materials, as well as whether they contain hydrogen (or water) or helium provides key information about how space weathering progresses in different phases and the relative rates of alteration.

We used focused ion beam microscopy (FIB) to prepare samples for analysis using an aberration-corrected Nion STEM equipped with detectors for electron energy loss spectroscopy (EELS) and energy dispersive X-ray spectroscopy (EDS). Spectrum image data cubes were collected in order to map changes in oxidation state, presence of volatiles, and elemental composition. FIB allows for preparation of site-selected regions of grains and allows us to maintain context and spatial relationships across phase boundaries and features of interest.

Using these methods, we have identified helium in vesicles in the rims of ilmenite grains from two different lunar soils. Figure 1 shows a small ilmenite grain attached to a larger plagioclase grain. The exposed surface of the ilmenite has a well-developed space weathered rim with $npFe^0$ inclusions and small vesicles. Planar defects are seen in this rim up to 135 nm from the surface. In comparison to a rim on an ilmenite grain from sub-mature lunar soil 71501 [2], the defects in the rim have high areal density. As was noted for that grain, helium implanted by the solar wind can be identified in some vesicles using EELS. The energy of the helium K-edge measured for these vesicles, 22.8 eV, is consistent with $n_{He} \sim 40\ nm^{-3}$, similar to what was seen in [2]. Thus far, helium has been identified only in vesicles or defects in oxides, not silicates, from the Moon.

Figure 2 shows scanning electron microscope (SEM) images of the surface of a multi-phase lunar grain. As noted for some Itokawa particles [4], the two phases show different surface morphology features, including blisters present on the Mg-, Fe-rich silicate phase (either olivine or pyroxene) but not the Al-rich (plagioclase) surface. The number of small (<100 nm) adhered spherical particles is also higher on the mafic grain. FIB/STEM can be used to determine if these blisters indicate the presence of vesicles and how the rim differs between these two phases across this boundary, as well as if any volatiles remain trapped in the vesicles.

The careful work on the Itokawa particles examined to date have shown the significant scientific value in each single grain through detailed comparisons with other grains, both asteroidal and lunar. Understanding how and when hydrogen and helium implanted by the solar wind coalesce into larger defects and vesicles requires an understanding of which phases host the most vesicles, whether or not there are other features associated with these vesicles, and what other processes, such as heating, might be necessary for vesicle formation. Detailed comparisons between samples from the Moon and from Itokawa will allow for a better understanding of how location in the Solar System may affect vesicle formation and volatile trapping and how the important space weathering processes vary between those locations.

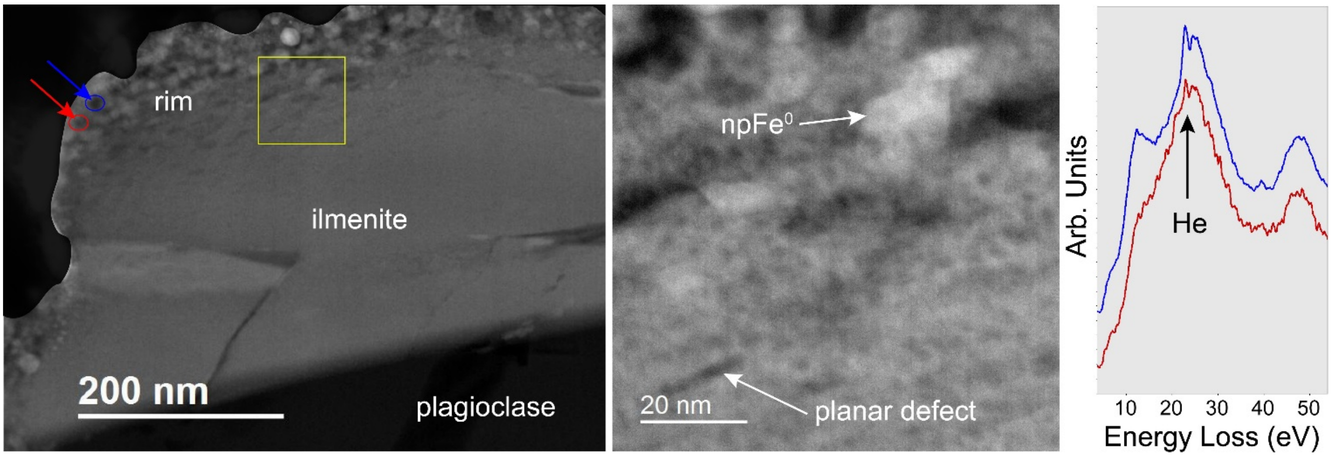

Figure 1. An ilmenite grain attached to a plagioclase grain in mature lunar soil 79221 has a well-developed space weathered rim on the exposed surface. Some of the vesicles in the rim contain trapped helium from the solar wind that can be measured using EELS.

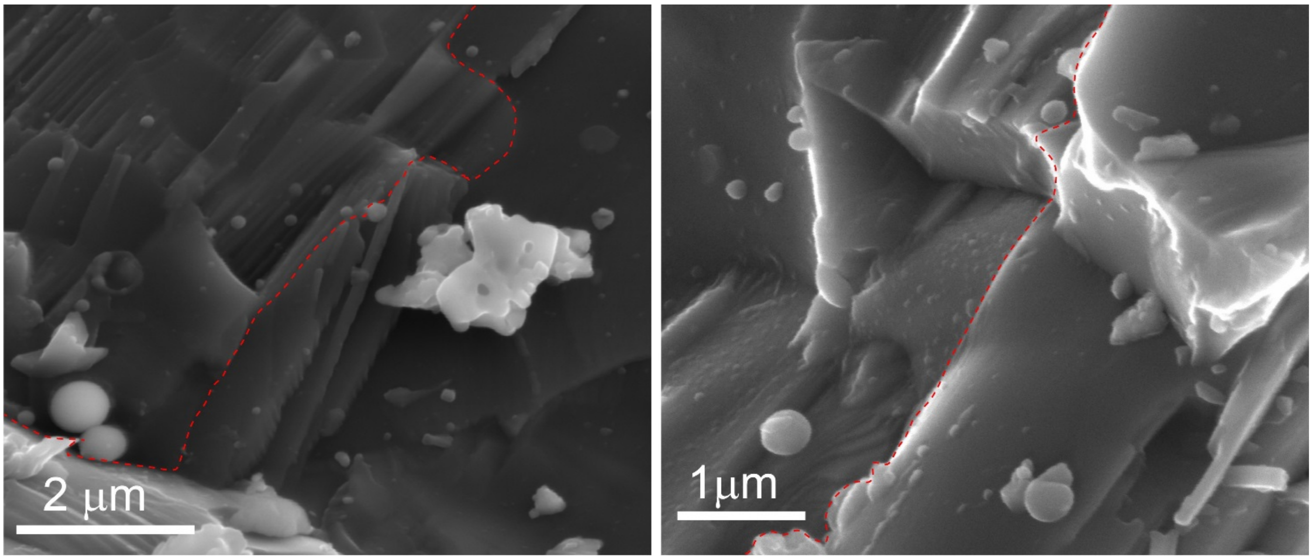

Figure 2. Different phases react very differently to the same space weathering exposure and thus are likely to have different rates of vesicle formation or have vesicles from through different mechanisms. (a) SEM secondary electron image shows the Mg-rich phase (left) is fractured in a different pattern than the Al-rich phase (right) and has more <100 nm adhered surface nanoparticles. (b) The Mg-rich silicate has numerous apparent blisters, while the Al-rich silicate lacks the blister-like features.

References

[1] Pieters, C.M., and S.K. Noble (2016) *JGR*, *121*, 1865.
[2] Burgess, K.D., and R.M. Stroud (2018) *GCA*, *224*, 64.
[3] Thompson, M.S., et al. (2016) *M&PS*, *51*, 1082.
[4] Matsumoto, T., et al. (2016) *GCA*, *187*, 195.

Preliminary results from sulfide Hayabusa particle RB-CV-0234

Devin L. Schrader[1] and Thomas J. Zega[2]

[1]*Center for Meteorite Studies, School of Earth and Space Exploration, Arizona State University, Tempe, AZ 85287-1404, USA (devin.schrader@asu.edu),*

[2]*Lunar and Planetary Laboratory, University of Arizona, Tucson, Arizona 85721, USA (tzega@lpl.arizona.edu)*

Introduction: We performed initial analyses of the sulfide Hayabusa particle RB-CV-0234, and compared it to our results from LL3–6 chondrite sulfides [1,2], with the goal of further constraining the formation and alteration conditions of asteroid Itokawa. Preliminary analysis by JAXA's Hayabusa examination team via scanning electron microscope (SEM) determined that RB-CV-0234 (25.9 µm in diameter) consists of FeS, Fe, FeNiS, and CuS, making it an ideal target potentially containing both pyrrhotite group sulfides [$(Fe,Ni,Co,Cr)_{1-x}S$] and the rare Ni-rich sulfide, pentlandite [$(Fe,Ni,Co,Cr)_{9-x}S_8$].

Sulfides are important to study as their compositions, textures, and crystal structures can be used to constrain oxygen fugacity of formation, shock stage, and aqueous-, thermal-, and cooling-histories [e.g., 3–8]. The pyrrhotite group sulfides are largely nonstoichiometric and have a range of compositions ($0<x<0.125$) and distinct crystal structures (polytypes). The stoichiometric end members are 2C (troilite; FeS, hexagonal) and 4C (Fe_7S_8, monoclinic) pyrrhotite. There are also pyrrhotites of intermediate compositions with $0<x<0.125$ (all hexagonal); including the non-integral NC-pyrrhotites and the integral 5C (Fe_9S_{10}), 6C ($Fe_{11}S_{12}$), and 11C ($Fe_{10}S_{11}$) pyrrhotites [e.g., 9–11]. Geothermometry of pyrrhotite-pentlandite intergrowths in meteorites shows that most formed via primary cooling from high temperature or thermal metamorphism [e.g., 12–14]. Sulfides in the LL4 to LL6 chondrites typically equilibrated between 600 and 500°C, consistent with formation during cooling after thermal metamorphism [14]. However, geothermometry of pyrrhotite-pentlandite intergrowths from an LL5–6 impact melt-breccia indicated that the sulfides were annealed at ≤230°C, likely after an impact event [12]. Analyses of Hayabusa particles have identified asteroid 25143 Itokawa as LL4–6 chondrite material (~10% LL4 and ~90% LL5–6) [e.g., 15–18] that was thermally metamorphosed between ~780 and 840°C [15]. Itokawa particles were found to record shock stages between S2 and S4, with most particles around S2 [19,20]. Sulfides in Hayabusa particles [e.g., 15,21,22] may record additional and/or complementary information on the formation conditions of asteroid Itokawa.

Samples and Analytical Procedures: We mounted RB-CV-0234 on an epoxy bullet, following the methods of [21], and microtomed the sample in preparation for analysis and sample extraction using the FEI Helios NanoLab 660 focused-ion-beam-SEM (FIB-SEM) at the University of Arizona (UAz). The visible particle surface was 25.0 × 10.2 µm after microtoming. X-ray element maps and high-resolution images of the microtomed RB-CV-0234 were obtained with the FIB-SEM prior to extraction of a ~12.4 × 11.2 µm section from one end of the whole particle, which was then thinned to electron transparency (<100 nm) following the methods of [23]. The FIB section was then analyzed using the 200 keV aberration-corrected Hitachi HF5000 scanning transmission electron microscope (TEM) at UAz.

Results: FIB-SEM X-ray element maps showed that the microtomed surface of RB-CV-0234 consisted entirely of pyrrhotite. However, X-ray element maps of the extracted FIB section, determined via TEM analysis, revealed a grain of pentlandite (4.8 × 1.3 µm) at the bottom of the section (**Fig. 1**). The FIB section contains a single large grain of pyrrhotite and a single smaller grain of pentlandite. Selected-area electron-diffraction (SAED) patterns of the pyrrhotite and pentlandite grains index to 2C pyrrhotite (troilite) and pentlandite along the [110] zone axis (i.e., they are crystographically oriented), respectively.

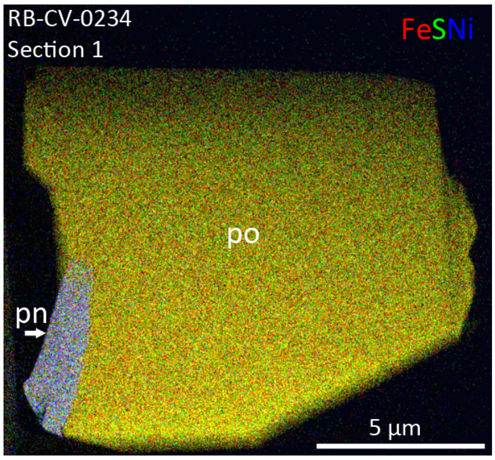

Fig. 1. Composite TEM X-ray element map (RGB=FeSNi) of RB-CV-0234 FIB Section 1; where po = pyrrhotite and pn = pentlandite.

Discussion: The preliminary results from the first FIB section from RB-CV-0234 are most consistent with it being a sulfide from an LL6 chondrite, similar to the sulfides from Saint-Séverin studied by [1]. We infer this because, based on results from the LL3–6 chondrite sulfides we previously studied via FIB-TEM [1,2], only sulfide grains in Saint-Séverin (LL6, S2 [24]) contain a similar pentlandite/pyrrhotite morphology (i.e., blocky pentlandite in pyrrhotite) and 2C pyrrhotite (troilite) with pentlandite [1]. The other LL chondrites we studied contained either a distinct morphology (e.g., pentlandite lamellae) and/or multiple polytypes of pyrrhotite [1,2]; perhaps indicating higher degrees of shock as troilite in ordinary chondrites is known to display shock indicators, such as fizzed and polycrystalline troilite [e.g., 8]. This conclusion is consistent both with the petrographic types represented in Hayabusa particles (10% LL4 and 90% LL5–6 [15,17,18]) and the most likely shock stage of Hayabusa samples (S2; [19,20]). Additional planned FIB section extractions from RB-CV-0234 will allow us to test this conclusion and investigate if the sulfide contains any evidence of space weathering [e.g., 22]. We plan to determine the compositions of both the pentlandite and the pyrrhotite via quantitative energy-dispersive X-ray spectroscopy with the TEM at UAz [25], and determine the sulfide's geothermometry to constrain its thermal history (i.e., if the sulfide was annealed at low temperature, or cooled from high temperature [e.g., 12,14]).

Acknowledgements: We thank JAXA for the loan of the Hayabusa particle used in this study through the 5th International Announcement of Opportunity, and NASA grant NNX17AE53G (DLS PI, TJZ Co-I) for funding this research.

References

[1] Schrader D. L. and Zega T. J. 2017. Abstract #6347. 80th MetSoc. [2] Schrader D. L. and Zega T. J. 2018. Abstract #2621. 49th LPSC. [3] Arnold R. G. 1967. Can. Min. 9:31. [4] Kissin S. A. and Scott S. D. 1982. Econ. Geol. 77:1739. [5] Raghavan V. 2004. J. Phase Equilib. 25:373. [6] Wang H. et al. 2006. J. Sulfur Chem. 27:1. [7] Harries D. and Langenhorst F. 2013. Meteorit. Planet. Sci. 48:879. [8] Bennet M. E. and McSween Jr. H. Y. 1996. Meteorit. Planet. Sci. 31:255. [9] Morimoto N. et al. 1975. Econ. Geo. 70:824. [10] Wang H. et al. 2006. J. Sulfur Chem. 27:1. [11] Harries D. et al. 2011. Am. Min. 96:716. [12] Jamsja N. and Ruzicka A. 2010. Meteorit. Planet. Sci. 45:828. [13] Schrader D. L. et al. 2015. Meteorit. Planet. Sci. 50:15. [14] Schrader D. L. et al. 2016. Geochim. Cosmochim. Acta 189:359. [15] Nakamura T. et al. 2011. Science 333:1113. [16] Noguchi T. et al. 2014. Earth, Planets, and Space 66:124. [17] Tsuchiyama A. et al. 2011. Science 333: 1125. [18] Tsuchiyama A. et al. 2014. Meteorit. Planet. Sci. 49:172. [19] Noguchi T. et al. 2011. Science 333:1121. [20] Zolensky M. E. et al. 2012. Abstract #1477. 43rd LPSC. [21] Berger E. L. and Keller L. P. 2015. Microscopy Today 23:18. [22] Harries D. and Langenhorst F. 2014. Earth, Planets, and Space 66:163. [23] Zega T. J. et al. 2007. Meteorit. Planet. Sci. 42:1373. [24] Rubin A. E. 2004. Geochim. Cosmochim. Acta 68:673. [25] Zega T. J. et al. 2018. Abstract #2084. Microsc. Microanal. 24 (Suppl. 1).

Exploring the potential of Xe^+ Plasma FIB for minimum mass-loss sectioning of meteoritic analogs of coarse-grained (0.2-1 mm) asteroidal samples from the JAXA Hayabusa 2 sample return mission to asteroid Ryugu.

A.J. Brearley[1], R.H. Jones[2], T. L. Burnett[3], J. Donoghue[3], and T. Nakamura[4]

[1]*Department of Earth and Planetary Sciences, 1University of New Mexico, Albuquerque, NM 87131, USA*
[2]*School of Earth and Environmental Sciences, University of Manchester, Oxford Road, M13 9PL, UK*
[3]*School of Materials, University of Manchester, Oxford Road, M13 9PL, UK*
[4]*Department of Earth and Planetary Materials Science, Tohoku University, Aramaki, Aoba, Sendai, Miyagi 980-8578, Japan.*

Introduction: The JAXA Hayabusa 2 sample return mission will collect samples of Ryugu, a spectral type Cg asteroid, in autumn 2018 and return them to Earth in December 2020. It is expected that a significant component of the material collected will be regolith particles that are ~0.2-1 mm in diameter. These comparatively large carbonaceous chondrite fragments will be the focus of research of the Coarse-grained Sample Analysis Team. Samples in this size range present significant challenges for sample preparation. It is highly desirable that the samples can be cut into two or more subsamples for analysis using different techniques, while leaving material that can be archived for future study. Typical cutting techniques such as wafering saws using wires or blades are highly wasteful in terms of mass. In preparation for these challenges, we are exploring the application of Xe^+ plasma FIB (P-FIB) techniques as a potential methodology for sectioning coarse-grained Hayabusa 2 particles, with minimum mass loss.

Background: Focused ion beam techniques have become the method of choice for the site-specific sample preparation of a wide range of synthetic and natural materials. Ga^+ FIB has become an established tool for the preparation of small volume samples for cross sectional imaging and TEM analysis [1]. However, the relatively low beam currents which can be obtained from Ga^+ ion sources limit their ability to section materials that are more than a few 10s of microns in size. The more recent development of P-FIB technology utilizing Xe^+ ions, delivers much higher beam currents and enhanced sputtering rates (10-30% higher and up to 300% for some materials [2]), has revolutionized the field of large area cross-sectional analysis, as well as enabling the extraction of large volumes of material for ex-situ analysis.

Methodology: A Thermo Fisher Dualbeam® Xe^+ P-FIB at the University of Manchester was used as a proof of concept instrument for our preliminary studies. A sample of the Murray CM2 chondrite was used as an analog material with properties that are likely to be a good match to samples that will be returned by the mission. Murray is a complex, heterogeneous meteorite with materials of diverse densities and grain sizes that sputter at different rates and represent a significant challenge. A chip of Murray, ~1x2 mm in size, was secured to an aluminium SEM stub using Superglue and was examined uncoated in the P-FIB.

Results: The first order sputtering behavior of Murray was determined by carrying out a cleaning cross section on a relatively flat surface of the sample. At instrumental conditions of 30 kV, 0.47 µA, a 50 x 50 μm^2 cleaning cross section depth of 30 µm (the calculated cutting depth for Si) sputtered to a measured depth of ~56 µm in 2 minutes. Sample sputtering was quite homogeneous across the whole area, except for an inclusion with much lower sputtering rates that was removed after a second cleaning cross section. A satisfactory surface was produced in approximately 3 minutes. A second experiment was performed to determine the viability of cutting larger regions of sample. A regular cross section was set up on the edge of the fragment with dimensions 316 µm (L), 66 µm (W) and 120 µm (D). Using a beam current of 1.3 µA, the pattern cut through to a depth of ~192 µm in 30 minutes (Fig. 1A). A sputter-resistant particle remained in the lower part of the surface that required three additional cleaning cross sections to reduce in size. These experiments show that sputtering is remarkably fast over large areas, even in regular cross section patterning mode, where the tip of the ion beam is removing material.

In order to section a single, coarse-grained particle, a complete cut across the entire diameter of the particle that maximizes the depth to width ratio of the cut is required. Due to increased re-deposition as the ion beam penetrates deeper into the sample, the sputtering rate will decrease with depth and the width of the cut will also become smaller. We explored two different approaches to cutting the sample to maximize the depth to width ratio of the trench. In the first case, a rectangular pattern 50 µm long, 5 µm wide and 30 µm deep was run at a beam current of 470 nA (40 seconds duration) on a relatively flat region of the sample surface. A regular cross section cut normal to the first rectangular pattern was then run to look at the geometry of the trench, which was carrot-shaped with a poor depth to width ratio of 2:1 (Fig. 1B, trench 1). A slight improvement in the depth to width ratio was obtained if the trench was open at one end at the start of the pattern (Fig. 1B, trench 2). This result demonstrates that sputtering using a standard rectangular pattern is inefficient and not a viable approach for sectioning this kind of chondritic material. An alternative approach is to take advantage of the higher sputtering rates when the ion beam interacts with the sample at glancing angle and sputtering occurs at the edge of the beam. For this experiment, we utilized a cleaning cross section pattern, but with dimensions that are essentially the reverse of those used typically for polishing a sample surface, i.e. the face that the beam is cutting is very narrow, but the pattern is highly elongate. A pattern with a width of 5 µm (on the cutting face), a depth of 50 µm and a length of 50 µm resulted in a trench in the sample with a depth to surface width ratio of ~9 (90 µm deep) (Fig. 1B, trench 3) in 40 seconds.

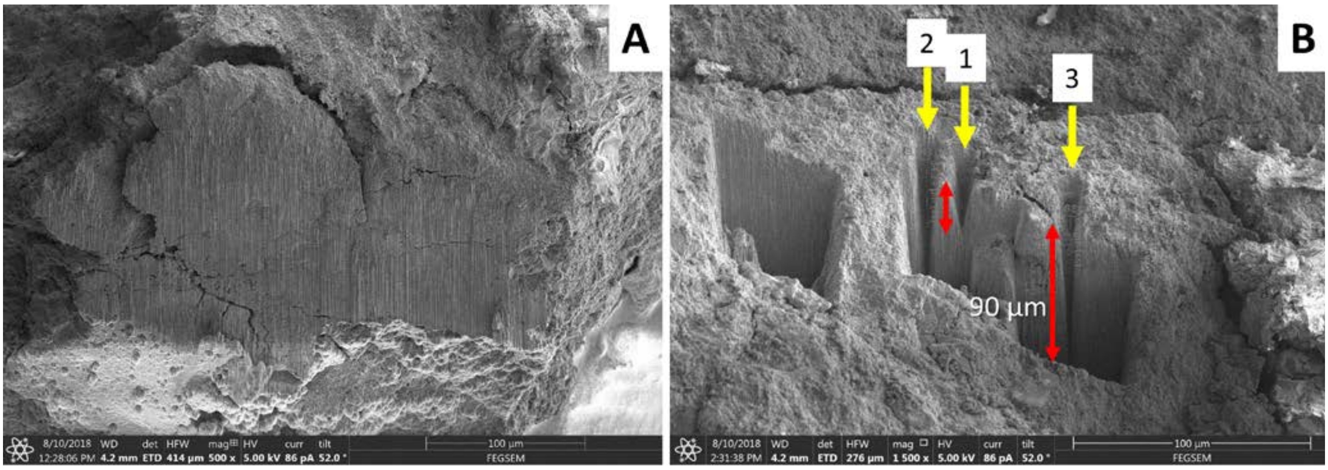

Figure 1 - A) SE image of Xe P-FIB cross section cut on the surface of a fragment of the Murray CM chondrite. The face is over 300 µm in width. B) SE image of trenches cut into Murray sample using different types of patterns. Trench 1 was cut using a rectangular pattern with closed ends that produced a carrot-shaped cross section. Trench 2 was cut using the same pattern, but the trench was open at one end resulting in a deeper trench. Trench 3 was cut using a narrow cleaning cross section, producing a deeper trench with improved depth to width ratio.

Conclusions: Although we have yet to cut an entire particle, these experiments demonstrate that P-FIB has great potential for sectioning Hayabusa 2 particles. Preliminary results show that it should be possible to section 500 µm diameter particles in time periods of ~1-2 hours. However, the heterogeneity of the sample in terms of sputtering rates does require that cutting through more resistant phases must be factored into the milling time. It may be advantageous sectioning the sample in two separate cuts run from opposite sides of the particle. Based on the depth to width ratio (9:1) obtained from the sample of Murray cut using a cleaning cross section, we estimate that the width of the top of the cut would be around 50 µm. Cutting particles larger than 500 µm in diameter in half would be more challenging and time consuming. A better strategy may be to remove serial slices of lower diameter. We are continuing to develop this method, including assessment of the extent of beam damage to the sample, adjacent to the cut.

References: [1] L.A. Giannuzzi, and F.A. Stevie (1999) Micron, 30, 197-204. [2] Burnett, T.L. et al. (2016) Ultramicroscopy 161, 119-129.

Thermal Infrared Spectra of Heated CM and C2 Chondrites and Implications for Asteroid Sample Return Missions

Helena Bates[1,2], Kerri Donaldson Hanna[2], Ashley King[1], Neil Bowles[2], Katie Rhodes[3] and Sara Russell[1]
[1]*Earth Science Department, Natural History Museum, London, SW7 5BD, UK*
[2]*Atmospheric, Oceanic and Planetary Physics, University of Oxford, Oxford, OX1 3PU, UK*
[3]*Earth Science and Engineering, Imperial College, London, SW7 5BB, UK*

Introduction: JAXA's Hayabusa2 arrived at its target asteroid, the C-type asteroid Ryugu, in June 2018 and NASA's Origins, Spectral Interpretation, Resource Identification and Security Regolith Explorer (OSIRIS-REx) is on its approach to its target, the B-type asteroid Bennu, with arrival due in December 2018. The C- and B-type asteroids are part of the larger C-complex class [1,2], which have been linked to carbonaceous chondrite meteorites, in particular the aqueously altered CM and CI chondrites [3–5]. These meteorites are rich in organics and water, and are considered chemically pristine, so investigating them and their parent body asteroids will tell us about the early evolution of our Solar System.

Some aqueously altered CM and CI chondrites have also experienced thermal metamorphism [6,7]. Previous work has suggested that thermally metamorphosed CM and CI chondrites could be good analogues for the C- and B-type asteroids [8–10] including Ryugu [11,12]. The surfaces of C-complex asteroids might contain a mixture of hydrated and dehydrated materials having experienced a complex history of both fluid and thermal alteration. Unravelling the effects of these processes will be imperative for putting data from Hayabusa2 and OSIRIS-REx into geologic context.

OSIRIS-REx and the Mobile Asteroid Surface Scout (MASCOT) on board Hayabusa2 both carry thermal infrared (TIR) instruments in order to determine surface mineralogy, the OSIRIS-REx thermal emission spectrometer (OTES) and the Mascot Radiometer (MARA). TIR spectra have many diagnostic spectral features associated with rock forming minerals [13]. These include the Christiansen feature (CF), between 7.5 – 9 μm, which is an emissivity maximum diagnostic of composition [13], the reststrahlen bands (RB), which are the fundamental vibrations of silicate minerals between 8 – 12 μm and 15 – 25 μm, and the transparency feature (TF), which is an emissivity minima between 11 – 13 μm caused by volume scattering in optically thin minerals [13]. Laboratory measurements in the TIR are generally made under ambient conditions; however previous work has shown that measuring under the appropriate near-surface asteroid conditions causes shifts in the position of the CF, and increases the spectral contrast between the CF and RBs [14–16]. Therefore, in order to accurately compare between laboratory measurements and data collected from asteroids, it is critical to perform measurements under simulated asteroid environment conditions (SAE).

Here we present TIR emissivity measurements, collected under ambient and SAE conditions, for a number of thermally metamorphosed CM and C2 chondrites. These SAE measurements should be more directly comparable to observations by OSIRIS-REx and Hayabusa2. There have been limited studies of TIR spectra measured under SAE for carbonaceous chondrites [16], and none on thermally metamorphosed CM and CI chondrites, so this offers a new opportunity to investigate the spectral signatures of Bennu and Ryugu.

Samples: Nakamura (2005) defined a heating scale for thermally metamorphosed CM and CI chondrites, from stage I to stage IV. Stage I samples have been heated to peak metamorphic temperatures of <250 ^{o}C, and show little to no dehydration of hydrous phases. Here we have investigated the sample MacAlpine Hills (MAC) 87300, an ungrouped C2 chondrite which previous work has suggested is a stage I sample, but shows CM and CO affinities [6,17]. Stage II samples have been heated to temperatures of 300 – 500 ^{o}C, and are mostly composed of a highly disordered phase thought to be dehydrated phyllosilicates. We investigated the CM2 Elephant Moraine (EET) 92069, and the anomalous CM chondrite Wisconsin Range (WIS) 91600, both of which have been suggested to be stage II samples [7,18]. We did not study any stage III samples, which have been heated to temperatures of 500 – 750 ^{o}C and show some recrystallization of anhydrous phases, but we did investigate the CM2 chondrites Pecora Escarpment (PCA) 02010 and PCA 02012, which are stage IV samples [19]. Stage IV samples have been heated to >750 ^{o}C and have experienced widespread recrystallization of anhydrous phases such as olivine and metal.

Experimental: TIR emissivity measurements were made under ambient and SAE conditions in the Planetary Analogue Surface Chamber for Asteroid and Lunar Environments (PASCALE) within the Planetary Spectroscopy Facility at the University of Oxford [16]. Under ambient conditions the sample was heated from below to ~80 ^{o}C whilst the chamber was held at an ambient pressure (~1000 mbar N_2) and temperature (~28 ^{o}C). Under SAE conditions, the near surface environment of Bennu is simulated by removing atmospheric gases from the chamber so measurements are completed under vacuum (<10^{-4} mbar), cooling the interior of the chamber to <-150 ^{o}C using liquid N_2 and heating the samples from above and below until the maximum brightness temperature of the sample is ~75 ^{o}C. This induces a thermal gradient in the upper hundreds of microns of the sample, which is what we would expect on the surface of Bennu near local midday. Spectra were collected using a Bruker VERTEX 70v Fourier Transform Infrared (FTIR) spectrometer at a resolution of 4 cm^{-1} from 1800 – 200 cm^{-1} (5.5 – 50 µm).

Results: Emissivity spectra are presented in Figure 1. The stage IV PCA 02010 and PCA 02012 samples are spectrally similar with the main diagnostic features located at similar wavelengths, and show a feature near 6 µm, which is not present in the stage II samples. This could indicate it is representative of the higher abundances of anhydrous phases in the stage IV samples. The spectra show a steep spectral contrast leading up to the CFs, which are identified near 8.5 µm, and emissivity maxima near 9.7 µm. The TFs for the stage IV samples are identified near 12.5 µm.

The spectral shapes of EET 96029 and MAC 87300 are also similar to each other, with CFs identified near 8.7 µm with additional emissivity maxima near 9.7 µm, and TFs at 12.5 µm. The similarity between EET 96029 and MAC 87300 requires further investigation, as they not only are classified differently, but also have different thermal histories.

The spectrum of WIS 91600 is different from the other meteorites investigated here. It has a broad emissivity maximum centred near 6.5 µm followed by an emissivity minima, and a CF near 9.4 µm. The CF at longer wavelengths suggests it is dominated by a different mineralogy in comparison to the other meteorites investigated here. Its TF is identified at similar wavelengths to the other samples near 12.5 µm. The spectra suggests WIS 91600 has a distinct mineralogy when compared with the other stage II samples, and further investigation into its composition is required to determine which mineralogy is dominating the spectra.

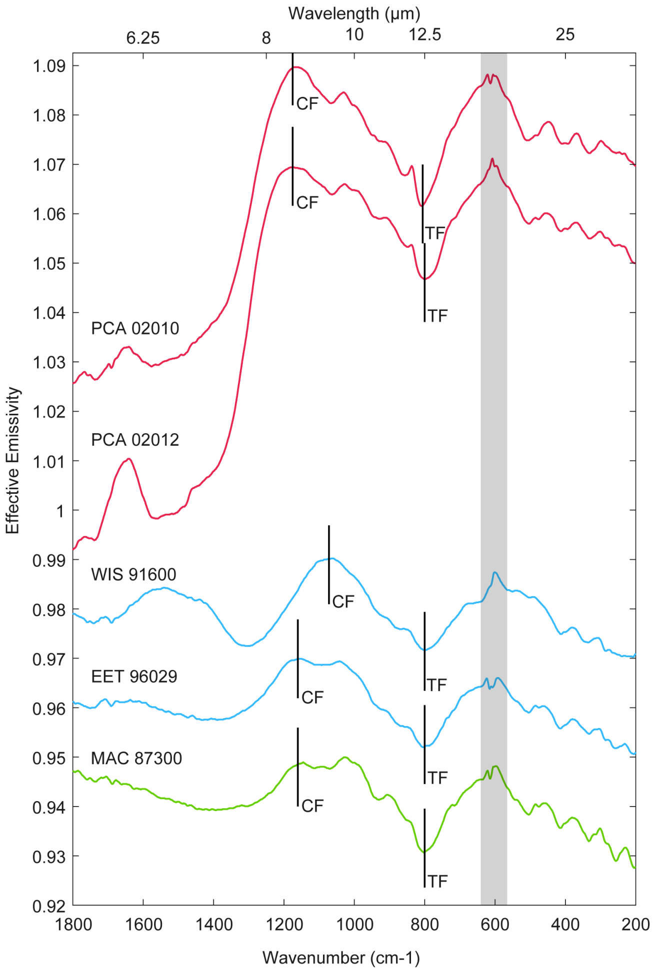

Figure 1: Emissivity spectra for the thermally metamorphosed CM and ungrouped chondrites investigated here. Green spectra are stage I, blue spectra are the stage II samples and red spectra are the stage IV samples. Data are normalized to unity and offset for clarity. The positions of the CF and TF are indicated. The grey box near 600 cm^{-1} indicates noise related to poor signal-to-noise resulting from the beam splitter.

There are clear spectral differences between samples that have been heated to different peak metamorphic temperatures. In order to better investigate these differences, exact mineralogy for each sample is necessary, so specific features can be tied to known compositions. Position-sensitive detector X-ray diffraction (PSD-XRD) is a method that has been used to determine modal mineralogy for a number of CI, CM, CV and CR chondrites [20–24]. It is able to directly detect all crystalline phases, and additionally investigate the presence of non-crystalline phases. Further studies are planned to obtain the PSD-XRD patterns for the exact samples used in this study, so modal mineralogy can be established and linked with our lab spectral measurements.

References

[1] DeMeo F.E. et al. 2009 Icarus 202:16 [2] Tholen D.J. 1984 [3] Burbine T.H. et al. in 2002 Asteroids III 653. [4] Licandro J. et al. 2007 Astronomy & Astrophysics 461:751.[5] Vilas F. et al. 1994 Icarus 109:274. [6] Nakamura T. 2005 Journal of Mineralogical and Petrological Sciences 100. [7] Tonui E.K. et al. 2014 GCA 126:284. [8] Clark B.E. et al. 2010 Journal of Geophysical Research: Planets 115. [9] Hiroi T. et al. 1993 Science 261:1016. [10] De León J. et al. 2012 Icarus 218:196. [11] Perna D. et al. 2017 A&A 599. [12] Moskovitz N.A. et al. 2013 Icarus 224:24. [13] Salisbury J.W. in 1993 Remote Geochemical Analysis 79. [14] Donaldson Hanna K.L. et al. 2012 Journal of Geophysical Research: Planets 117. [15] Thomas R. et al. 2014 45th LPSC [16] Donaldson Hanna K.L. et al. 2017 48th LPSC [17] Sears D.W.G. et. al. 1990 21st LPSC [18] Lee M.R. et al. 2016 GCA 187:237. [19] Alexander C.M.O. et al. 2013 GCA 123:244. [20] Howard K.T. et al. 2009 GCA 73:4576. [21] Howard K.T. et al. 2010 GCA 74:5084. [22] Howard K.T. et al. 2015 GCA 149:206. [23] King A.J. et al. 2015 GCA 165:148. [24] King A.J et al. 2015 Meteoritics & Planetary Science 50:A194.

The Jbilet Winselwan CM chondrite: an analogue for C-type asteroid sample return

Ashley J. King[1], Paul F. Schofield[1] and Sara S. Russell[1]
[1]*Department of Earth Science, Natural History Museum, London, SW7 5BD, UK*
E-mail: a.king@nhm.ac.uk

In June 2018 JAXA's Hayabusa-2 mission reached its target, the C-type asteroid Ryugu, and in December 2018 NASA's OSIRIS-REx spacecraft will arrive at the B-type asteroid Bennu. The C-complex class of asteroids have been linked to the carbonaceous meteorites, in particular the aqueously altered CI and CM chondrites, and are therefore expected to be chemically pristine and contain volatile and organic species [1]. A major aim for both missions is to collect and return to Earth samples from the asteroid surfaces in order to learn about the formation and evolution of the Solar System.

The Jbilet Winselwan meteorite was found on the 24^{th} May 2013 near Smara in Western Sahara, and with a total recovered mass of ~6 kg is currently the fourth largest CM chondrite (the largest find) [2]. Its bulk C, N and O isotopic compositions and major element abundances are within the range of other CM chondrites [2, 3]. Petrographic observations show that it consists of chondrules and calcium-aluminium-rich inclusions (CAIs, <1 vol%) surrounded by dusty rims and set within a matrix of phyllosilicates, oxides and sulphides [2–5]. Like many CM chondrites, Jbilet Winselwan is a breccia with distinct lithologies that underwent varying degrees of aqueous alteration [2–5]. In most lithologies the chondrules and CAIs are partially altered and the abundance of metal is low (<1 vol%), consistent with petrologic sub-types 2.7 – 2.4, whereas in others the chondrules and CAIs are completely altered suggesting more extensive hydration to petrologic sub-types ≤ 2.3 [2–5]. The brecciated nature of Jbilet Winselwan is also highlighted by variations in H_2O and carbonate abundances when analysing different aliquots of the meteorite [3].

Following aqueous alteration some lithologies in Jbilet Winselwan suffered a period(s) of thermal metamorphism. The matrix often has a "spongy" appearance and melted Fe-sulphide masses are present [4]. Bulk X-ray diffraction (XRD) indicates that the phyllosilicates are dehydrated to a highly disordered phase (~70 vol%) and the abundance of tochilinite, which breaks down at temperatures of ~120°C, is low relative to other CM chondrites [3]. Depletions of volatiles such as He and Cd in Jbilet Winselwan are consistent with a peak metamorphic temperature of 400 – 500°C [3]. However, Göpel et al. [6] found no depletions in volatile trace elements and not all of the phyllosilicates are dehydrated [2], suggesting that the heating was heterogeneous and did not affect all regions within Jbilet Winselwan equally.

The Jbilet Winselwan CM chondrite records a complex history of aqueous and thermal processing on a C-type asteroid. It is one of >20 CM chondrites identified as having experienced both hydration and thermal metamorphism [7]. Aqueous alteration took place when accreted ices melted on the parent body and reacted with the original anhydrous mineral assemblage. The presence of a dehydrated phyllosilicate phase in Jbilet Winselwan implies that thermal metamorphism occurred either simultaneously with, or more likely after, aqueous alteration had ceased. Mineral textures and organic structures in heated CM chondrites indicate that the metamorphism was short-lived, perhaps on the order of hours to several years, consistent with either impacts and/or solar radiation on asteroid surfaces [8]. We favour impacts because depending on the size, velocity and composition of the impactor and target rocks it could produce regions on the parent body with different thermal histories [9], as appears to be the case for Jbilet Winselwan.

Many of Jbilet Winselwan's key properties are similar to Y-793321, which is a sample of dehydrated regolith from the surface of a water-rich asteroid [10]. The visible and near-infrared (IR) reflectance spectra of Jbilet Winsewan, Y-793321 and other heated CM chondrites share a number of features with some low albedo, C-complex asteroids, including Ryugu [11, 12]. This suggests that the surfaces of C-complex asteroids are likely to host a diverse mixture of hydrated and dehydrated phases, and that heated CM chondrites such as Jbilet Winselwan are excellent analogues for the types of materials that will be encountered by the Hayabusa-2 and OSIRIS-REx sample-return missions.

References

[1] Cloutis E. et al. 2011. Icarus 216:309. [2] Ruzicka A. et al. 2015. M&PS 50:1662. [3] King A. et al. 2018. M&PS *in review*. [4] Zolensky M. et al. 2016. Abstract #2148. 47th LPSC. [5] Friend P. et al. 2018. M&PS *in press*. [6] Göpel C. et al. 2015. GCA 156:1. [7] Nakamua T. 2005. JM&PS 100:260. [8] Nakato A. et al. 2008. EP&S 60:855. [9] Bland P. et al. 2014. Nat. Comm. 5:5451. [10] Nakamura T. 2006. E&PSL 242:26. [11] Hiroi T. et al. 1993. Science 261:1016. [12] Vilas F. 2008. Astronom. J. 135:1101.

Sulfide mineralogy of heated CM/CI-like chondrites as indicator of asteroidal processes

Dennis Harries[1]

[1]*Friedrich Schiller University Jena, Institute of Geosciences, Carl-Zeiss-Promenade 10, 07745 Jena, Germany*
(dennis.harries@uni-jena.de)

Introduction. Thermal alteration of C-type asteroidal regoliths may induce mineralogical and spectral changes and is therefore of interest to ongoing missions such as Hayabusa2 or OSIRIS-REx. Heating effects superposed on earlier aqueous alteration of CM/CI-like chondrites have been described from multiple meteorites beginning in the late 1980s (e.g., [1], [2], [3]) and continue to be found and systematically classified into heating stages (HS I to IV with increasing temperatures [4]). Yet, it is not clear what kind of process is responsible for the thermal overprint and whether it specifically operated on CM/CI-like parent bodies or can be generally expected to affect asteroids and their regolith surfaces. Clearly, the hydrated mineralogy of CM/CI-like meteorites is highly susceptible to changes via thermal processes, and their effects, such as the amorphisation and recrystallization of phyllosilicates, can be readily observed. However, similar thermal events may go unnoticed in non-hydrated meteorite types due to a lack of suitable mineral indicators if heating persisted only for a relatively short time as indicated by CM/CI-like chondrites.

Sulfide minerals such as pyrrhotite ($Fe_{1-x}S$), troilite (FeS) and pentlandite [$(Fe,Ni)_9S_8$] are particularly sensitive to heating and, even before melting, may decompose by loss of sulfur and textural changes [5]. Therefore, they potentially may serve as an alternative indicator of thermal events not only for C-type asteroidal surfaces but also for S-type asteroids such as 25143 Itokawa visited by Hayabusa.

Samples and Methods. TEM studies of the sulfide mineralogies of Yamato (Y-)791198 (CM2, HS I), Y-793321 (CM2, HS II), Y-86720 (CM/CI-like, HS IV), Belgica (B-)7904 (CM-like, HS IV) have been described by [5] and will be summarized here. Additionally the meteorites Y-980115 (CI-like, HS II; [6]) and North West Africa (NWA) 11024 (CM-like, HS III/IV; [7]) have been investigated by SEM and TEM using FIB preparation. Study of the mildly heated CM2 chondrite Jbilet Winselwan (HS II;[8]) is ongoing.

Observations. Compared to the pristine Y-791198 the slightly heated regolith breccia Y-793321 [9] shows only subtle changes in sulfide mineralogy, mostly limited to increased grain sizes of exsolved pentlandite and troilite lamellae in pyrrhotite-bearing, former monosulfide solid solution (MSS) grains. Nanocrystalline phosphorus-bearing pentlandite, occasionally carrying chromium nitride in both meteorites [10] also shows an increase in grain size.

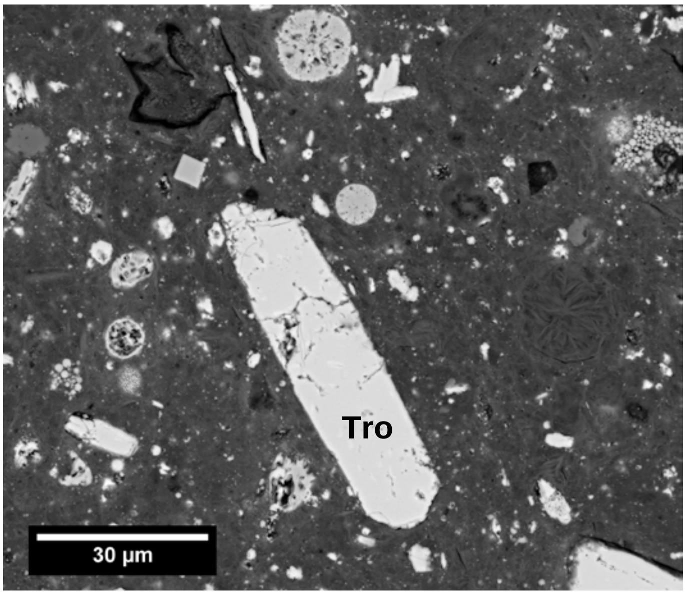

Figure 1. Euhedral sulfide crystals in Y-980115 are replacements of troilite (Tro) after hydrothermally formed pyrrhotite.

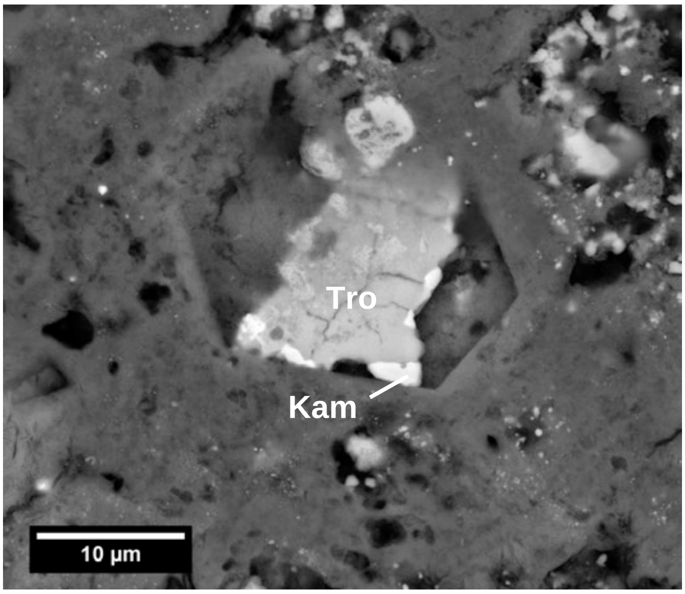

Figure 2. Formerly euhedral sulfide crystal in Y-86720 replaced by troilite (Tro) and partially converted to low-Ni kamacite (Kam).

Substantial mineralogical changes are observed in Y-86720 and B-7904, which contain almost exclusively troilite, which in part has been converted to low-Ni metallic iron (kamacite). Pentlandite appears to be absent in Y-86720, but B-7904 contains rare grains of Fe-rich pentlandite. Both contain small grains of Ni-rich metal (approaching 50 at% Ni in some cases).

Y-980115 shows a brecciated texture with internally fine grained clasts rich in phyllosilicates, magnetite and sulfides. The textures and particularly the morphology of magnetite and sulfide crystals are typical of CI chondrites. Large sulfides grains account for up to 2.8 vol% of the rock. Fe sulfide grains frequently show euhedral platelet shapes and reach sizes up to 70 µm. TEM-SAED patterns obtained from two apparently euhedral sulfide platelets extracted by FIB indicate that the sulfide is polycrystalline troilite and TEM imaging shows that the 'crystals' internally contain abundant grain boundaries meeting in 120° triple junctions. Pentlandite is present as internal grains within the platelets and SAED shows that it does not have a topotactic relationship with the surrounding polycrystalline troilite. The adjacent matrix is poorly crystalline but shows typical fibrous or scaly textures of phyllosilicates. EDS analyses of such aggregates indicate a typical serpentine composition, but SAED only showed diffuse rings with the larges *d*-value located at 0.465 nm. One better crystalline aggregate gave a diffraction pattern with largest *d*-value of 0.97 nm consistent with a talc group mineral; another showed polycrystalline rings consistent with olivine.

NWA 11024 displays typical fine-grained rims (FGRs) around chondrules. One rim sampled by FIB shows abundant Ni-rich metal grains < 1 µm in diameter with a composition centered about $Fe_{50}Co_3Ni_{47}$. The only present sulfide is troilite; Ni-poor metal and pentlandite are absent. The phyllosilicates originally present in the FGR have been converted to nanocrystalline olivine as indicated by SAED patterns. A second FIB obtained from a coarse phyllosilicate aggregate shows it to be a pseudomorph consisting entirely of nanocrystalline, Fe-rich olivine and minor amounts of Fe sulfide (probably troilite).

Discussion. The observations collected on a number of meteorites indicate that progressive thermal overprinting of CM/CI-like chondrites results in sulfur loss of pyrrhotite to form nearly stoichiometric troilite. Because pyrrhotite ($Fe_{1-x}S$) can be considered as an 'omission' solid solution between FeS and a hypothetical vacancy endmember VaS (Va = vacancy), the reaction can be written as $VaS \rightleftharpoons 0.5S_2$. Thus, sulfur loss progressively decreases the non-stoichiometry of $Fe_{1-x}S$ until FeS is reached. The preservation of pentlandite in Y-980115 suggests that it is stable at least until about this point. Further heating and increasing loss of sulfur probably leads to the decomposition of pentlandite to form Ni-rich metal as observed in NWA 11024. Preliminary thermodynamic calculations in the Fe-Ni-S system indicate that pentlandite with the composition $Fe_{4.5}Ni_{4.5}S_8$ is not stable with respect to $Fe_{50}Ni_{50}$ metal at temperatures above ~280 °C and a sulfur fugacity buffered by the presence of troilite. This needs further refinement for variable Ni/Fe ratios of pentlandite and the resulting metal. At highest temperatures troilite decomposes to form Ni-poor metal via the reaction $FeS \rightleftharpoons Fe + 0.5S_2$ as observed in B-7904 and Y-86720 of heating stage IV. Besides temperature the sulfur fugacity is therefore an important parameter that controls the decomposition. In all cases, the change of sulfide mineralogy requires at least partially open-system behavior such that S_2 (or H_2S) is lost from the rock, suggesting heating in a near-surface regolith or within a small meteoroid.

Potentially, the thermal decomposition of sulfide minerals can serve as another indicator of thermal processing on asteroid surfaces beside the dehydration of phyllosilicates. S-type chondritic regoliths that do not contain phyllosilicates may show heating effects by the presence of decomposed sulfides. However, the direct irradiation of sulfide surfaces by solar wind ions may produce similar effects at lower temperatures [11] and further investigations must establish differentiating criteria.

Acknowledgements. NIPR and S. Ebert/A. Bischoff/S. Wengert/S.Vasilev are gratefully acknowledged for providing the samples. This work was supported by the DFG (LA 830/14-1 to F. Langenhorst) and FSU Jena (DRM/2016-01).

References

[1] Akai, J. (1988) Geochim. Cosmochim. Acta, 52, 1593-1599. [2] Tomeoka, K. et al. (1989) Proc. National Institute of Polar Research Symposium on Antarctic Meteorites 2, 55-74. [3] Ikeda Y. (1992) Proc. National Institute of Polar Research Symposium on Antarctic Meteorites 5, 49-73. [4] Nakamura, T. (2005) J. Min. Pet. Science, 100, 260-272. [5] Harries, D. and Langenhorst F. (2013) Meteoritics & Planetary Science, 48, 879-903. [6] Kikuchi, K. et al. (2017) 8th Symposium on Polar Science/Antarctic Meteorites XXXX (abstract 00272). [7] Ebert, S. et al. (2018) submitted to Meteoritics & Planetary Science. [8] Nakamura T. et al. (2014) 5th Symposium on Polar Science/Antarctic Meteorites XXXVII (abstract 00315). [9] Nakamura, T. (2006) Earth and Planetary Science Letters. 242, 26-38. [10] Harries, D. et al. (2015) Nature Geoscience, 8, 97-101. [11] Matsumoto, T. et al. (2018) 81st Annual Meeting of The Meteoritical Society (abstract 6096).